MODELLING THE DC PERFORMANCE OF GAAS HOMOJUNCTION BIPOLAR TRANSISTORS

by

SOON PENG LEE

A THESIS SUBMITTED IN PARTIAL FULFILMENT OF
THE REQUIREMENTS FOR THE DEGREE OF
MASTER OF APPLIED SCIENCE

in

THE FACULTY OF GRADUATE STUDIES
DEPARTMENT OF ELECTRICAL ENGINEERING

We accept this thesis as conforming
to the required standard

THE UNIVERSITY OF BRITISH COLUMBIA

NOVEMBER, 1985

In presenting this thesis in partial fulfilment of the requirements for an advanced degree at the The University of British Columbia, I agree that the Library shall make it freely available for reference and study. I further agree that permission for extensive copying of this thesis for scholarly purposes may be granted by the Head of my Department or by his or her representatives. It is understood that copying or publication of this thesis for financial gain shall not be allowed without my written permission.

DEPARTMENT OF ELECTRICAL ENGINEERING

The University of British Columbia
2075 Wesbrook Place
Vancouver, Canada
V6T 1W5

Date: NOVEMBER, 1985

Abstract

Two models, one analytical and one numerical, have been developed to predict the dc performance of GaAs homojunction bipolar transistors. In each case the minority carrier properties of lifetime and mobility have been described by polynomial fits to recent data. Bandgap narrowing in the emitter and base regions has also been taken into account. The analytical model assumes uniform doping in the three regions of the transistor and is thus appropriate to predicting the performance of devices fabricated using epitaxial technologies. This model is also useful for carrying out sensitivity analyses. The importance of parameters such as regional widths and doping densities, minority carrier lifetimes and surface recombination velocity is examined here. The numerical model is useful for describing the performance of ion-implanted devices. Good agreement is obtained between results from the model and recent experimental data from prototype devices.

Table of Contents

List of figures

List of Figures

List of Figures

List of Tables

Acknowledgement

I would like to thank my supervisor, Dr. D. L. Pulfrey, for his continual guidance, support and encouragement during the course of this work.

I would also like to thank Dr. P. Van Halen for his help in developing the analytical model and Mr. D. Hui for his help in using the curve fitting routines on the HP 9816. Thanks are extended to Mr. D. S. Camporese and Mr. W. Tang for their many useful discussions.

1. INTRODUCTION

In recent years, there has been a growing interest in the use of gallium arsenide for integrated circuit applications. Because of its energy band structure, gallium arsenide exhibits some material properties which are superior to that of other semiconductors such as silicon and germanium. Its electron mobility is about 5-6 times higher than that of silicon, while its energy bandgap is about 1.43 eV, compared to 1.11 eV of silicon at room temperature. In addition, GaAs substrates are available in a semi-insulating form which substantially reduces the parasitic capacitances of electronic circuits, resulting in faster device speeds. Therefore, GaAs is suitable for a number of high frequency, high temperature applications, such as ultrahigh speed logic and signal processing, not presently realisable by silicon devices.

To date, most of the gallium arsenide circuits have been fabricated using MESFET (Metal Semiconductor Field Effect Transistor) technology. Complex large scale integrated circuits with a few thousand gates have been made. However, as the level of integration of GaAs circuits increases, some difficulty is encounterd with the FET technology. Logic circuits fabricated using depletion-mode MESFETs cannot contain more than 10,000 gates due to the large logic swing and 'normally on' characteristics of the D-MESFETs [1]. The latter could cause severe power dissipation problems. Although the enhancement-type MESFET

is normally off, its low logic swing (about 0.5 V) makes it difficult to control the device process parameters such as thickness and doping level in the transistor channel layer to the degree necessary to maintain a uniform pinch-off voltage. To obtain a good yield of devices at the VLSI level, the transistor's threshold voltage should not deviate more that five percent [2]; this would be very difficult to achieve with the E-MESFETs, since that translates into a pinch-off voltage variation of no more than 25 mV.

In view of these problems with MESFETs, one would like to consider the possibility of using bipolar technology for the fabrication of GaAs VLSI circuits. It is known that bipolar transistors offer several advantages over field effect transistors. The threshold voltage (the emitter-base bias voltage for some fixed collector current) of a bipolar transistor is relatively constant for a given bias, since it is mainly determined by the energy bandgaps of the emitter and base region of the device, rather than by the process parameters. A threshold variation of a few millivolts can be easily obtained in bipolar integrated circuits. Besides, bipolars are also known to have larger driving capability than field effect transistors, therefore they are more suitable for power device applications, or circuits with large fan-outs.

One of the possible choices for GaAs bipolar VLSI applications is the heterojunction bipolar transistor. Kroemer [3] has predicted that the heterojunction bipolars

exhibit a frequency response which is superior to that of FETs. A comparison by Eden [4] estimates that the gain-bandwidth product of a GaAs heterojunction bipolar transistor can be as high as 100-200 Ghz, while a MESFET with a gate length of 0.5 micron can only achieve about 30 Ghz. Despite this performance advantage enjoyed by the heterojunction bipolar transistors over the MESFETs, the complexity of their fabrication, which involves sophisticated Molecular Beam Epitaxy (MBE) techniques to grow the heterojunction, the use of ion-implantation for electrical isolation, the requirements of an extremely thin base layer (less than 100 nanometers) and small contact areas, has made the realisation of a large scale integrated circuit rather difficult at the moment. The GaAs homojunction bipolars, on the other hand, seem to offer a better perspective. The homojunction transistor fabrication process is simpler as only ion-implantations are employed to create the various doped layers as well as the isolation regions in the transistor structure. The ease of fabrication implies that homojunction bipolars should exhibit a higher yield in comparison to heterojunction bipolars.

GaAs homojunction bipolar transistors are generally thought to suffer an inherent design disadvantage that make them rather unfavourable in frequency response compared to the heterojunction bipolars. In order to maintain a high emitter injection efficiency in the homojunction bipolar, the base doping level has to be made only a small fraction

of the emitter doping level. The base region in a heterojunction bipolar, however, can be comparable in doping or even more heavily doped than the emitter region without affecting the injection efficiency, due to the heterojunction emitter that provides a large energy barrier to the emitter back-injected current. It is generally agreed that a heavily-doped base region reduces the base resistance, leading to substantially improved transistor frequency response. Recently, Tan and Milnes [5] have shown by their numerical study of the frequency response of the GaAs homojunction and heterojunction npn transistors that, if the parasitic base resistance is minimized in the homojunction bipolar transistor design, it is possible to achieve high speed operation in a GaAs homojunction bipolar that is comparable to that of a GaAs heterojunction bipolar. Therefore, it is deemed important to evaluate and investigate the operation and performance of the GaAs homojunction bipolar transistor in view of its vast potential.

The work on GaAs homojunction bipolar transistors began in the early 1960's. The first transistor was made by alloying a tin emitter to a diffused p-type base [6]. Succeeding devices were fabricated by using two-diffusion processes [7-11], or by employing vapour phase epitaxy methods [12]. The experimental results of these early devices were rather discouraging. In general, the static current gains obtained were quite low, and the frequency

gain-bandwidth products were typically in the range of a few hundred Mhz. In some cases, when devices with high gain were made, either they possessed very poor cutoff frequency [10], or they degraded within a short period of their fabrication [12]. The yield of these transistors was very low, due to the difficulty in controlling the required submicron base width by diffusion or epitaxial techniques. Not surprisingly, research into GaAs homojunction bipolar devices was discontinued for some time after these initial efforts.

The use of ion-implantation in semiconductor device fabrication and processing has brought a reprieve for the GaAs homojunction bipolar transistors. Precise control over the junction depth and the doping level in the various transistor regions can be achieved by adjusting the implant dose and energy. Recently, a number of ion-implanted GaAs homojunction bipolars have been made [13-19]. The successful development of planar vertical npn devices and lateral pnp transistors indicate the potential application of this bipolar technology in the Integrated-Injection Logic type of digital circuits. The current gains measured in these devices were typically in the range of 7-35; these were attributed to unspecified leakage currents at the surface. It has been suggested that this surface leakage effect can be reduced by incorporating a guard ring structure in the device design [20], thereby yielding higher transistor gains.

In view of these new experimental results, it was felt that a theoretical modelling of the GaAs homojunction bipolar would be very useful. The simulation of bipolar transistor behaviour should provide insightful information on the factors affecting the operation of an actual device. In addition, by studying the effect of varying device design parameters such as the doping levels in the emitter, base and collector regions, it should be possible to come up with a device design that provides optimum performance.

A number of problems are encountered in modelling GaAs bipolar devices. At present, there is a lack of knowledge of some properties of GaAs such as the doping dependence of mobility and recombination, the effects introduced by heavy doping and by surface states. In addition, the number of defects in GaAs are higher than that for elemental silicon, where antisite defects do not have to be considered. The presence of a large number of defects, together with the fact that the recombination mechanisms in bipolar devices are affected by the growth process of the substrate used, imply that the transistor characteristics will be material dependent. In the case of ion-implanted transistors, the effects of the implant mask, of the diffusion of dopants during thermal annealing, and the actual activation efficiency of implanted species on the carrier concentration profile have to be considered as well. In view of these uncertainties, it is very difficult to come up with a model that will give an exact prediction of the device behaviour

for a given operating condition. The approach that has been taken in the work described in this thesis seeks to incorporate the parameters pertaining to these effects into the model, and by making the appropriate assumptions, to predict theoretically the characteristics of particular bipolar transistors, and to correlate these to those observed experimentally. In this work we restrict ourselves to a study of the dc performance of GaAs homojunction bipolar transistors.

Two different models are developed to study the dc behaviour of GaAs bipolar homojunction transistors. An analytical model, which requires the assumption of uniform doping in the various transistor regions, is described in Chapter 2. A numerical model, which is based on the well-known SEDAN program [21], suitably modified to accommodate the parameters and properties of GaAs is described in Chapter 3. It is assumed in both models that the transistor is operating under low injection conditions. Also, only one-dimensional device structures are considered, since multi-dimensional effects are not profound when the driving currents are low. The use of two different models arises from the need to characterize transistor structures built by different fabrication techniques. In addition, the analytical model is useful in performing a sensitivity analysis on design parameters which affect device behaviour, while the numerical model is used to simulate the outputs of devices with non-uniform doping, such as those transistors

recently fabricated by ion-implantation [13-19].

2. THE ANALYTICAL MODEL

2.1 INTRODUCTION

In this chapter, an analytical model for the calculation of the DC characteristics of a GaAs homojunction npn bipolar transistor is described. This model has the advantage of using simple analytical, closed form expressions to relate the transistor current components to the bias conditions. It is used as a sensitivity test for studying the effect of the various device parameters such as minority carrier lifetimes, surface recombination velocity, regional doping and physical dimensions on the performance of the bipolar transistor. The doping levels in the emitter, base and collector regions of the transistor are assumed to be uniform, therefore this model is most suitable for characterising GaAs homojunction bipolar transistors built by epitaxial techniques such as LPE (Liquid Phase Epitaxy), VPE (Vapor Phase Epitaxy), or MBE (Molecular Beam Epitaxy).

The analytical model is a one-dimensional transistor model and the model parameters are those involving the physical properties of GaAs needed in the computations of the current components resulting from a certain applied bias. The description and formulation of the transistor model and the model parameters, together with the results and discussions are given in the subsequent sections of this chapter.

2.2 THE TRANSISTOR MODEL

For a one-dimensional, uniformly doped bipolar transistor, the device analysis can be performed by the classical Shockley regional approach, in which the transistor structure is divided into two depletion regions, and three charge-neutral regions. The various DC current density components in the device are calculated by solving the continuity equations and the current transport equations for a given set of boundary conditions. The current flows in the one-dimensional transistor structure are shown in Figure 2.1, where W_E, W_B and W_C are the widths of the neutral regions of the emitter, base and collector respectively. $(-X_E-W_E)$ and (W_C+X_C) represent the emitter and collector ends respectively.

The steady-state continuity equations for electrons and holes with no carrier generation are as follows:

$$\frac{d^2p}{dx^2} - \frac{p - p_n^o}{D_p \tau_p} = 0 \qquad (2.1)$$

$$\frac{d^2n}{dx^2} - \frac{n - n_p^o}{D_n \tau_n} = 0 \qquad (2.2)$$

The current transport equations in the neutral regions are given by:

$$J_n = qD_n \frac{dn}{dx} \qquad (2.3)$$

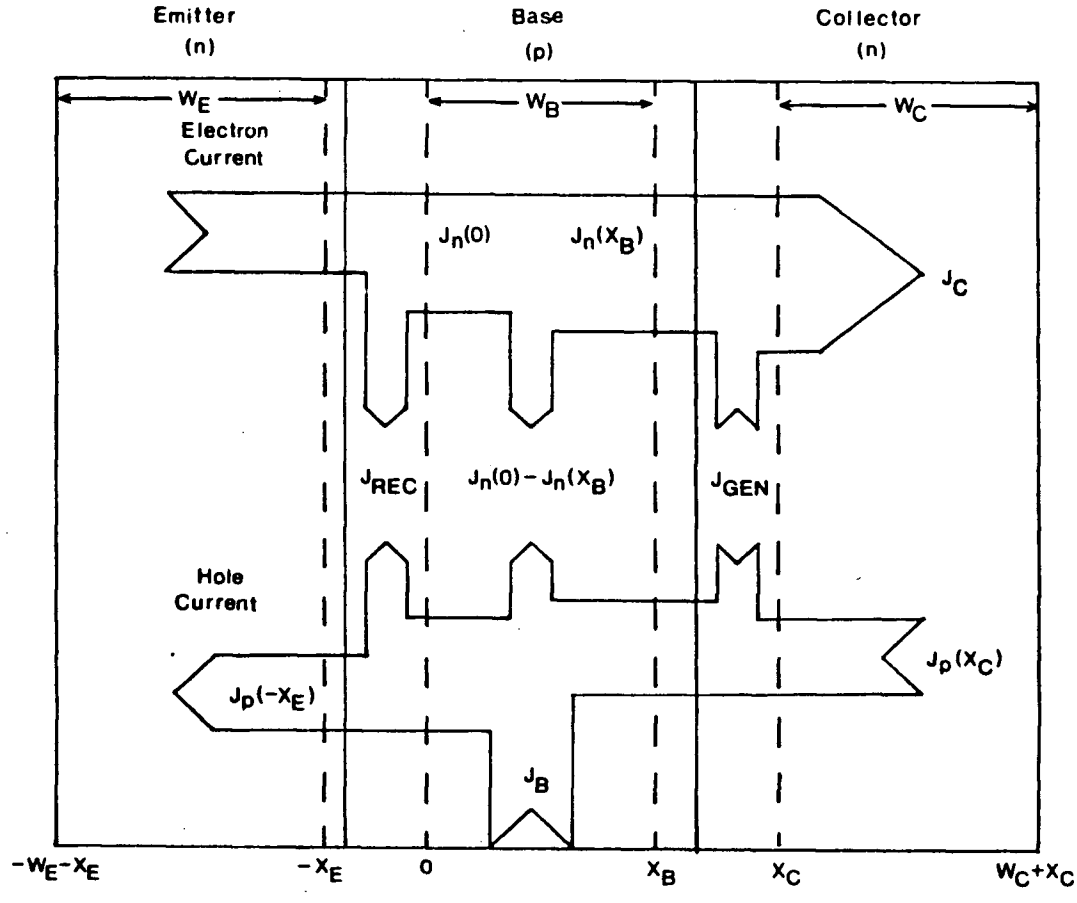

Fig. 2.1 Schematic of current flows in a homojunction bipolar transistor.

$$J_p = -qD_p \frac{dp}{dx} \qquad (2.4)$$

The currents consist of the diffusion component only, since there is no potential variation in a constantly doped semiconductor region to give rise to the drift term. By solving equations (2.1)-(2.4), the general solutions are derived as:

$$J_n = q \frac{D_n}{L_n} \left[A.\exp\left(\frac{-x}{L_n} \right) + B.\exp\left(\frac{+x}{L_n} \right) \right] \qquad (2.5)$$

$$J_p = q \frac{D_p}{L_p} \left[C.\exp\left(\frac{-x}{L_p} \right) + C.\exp\left(\frac{+x}{L_p} \right) \right] \qquad (2.6)$$

where q is the electronic charge, D_n and D_p, τ_n and τ_p, L_n and L_p are the diffusion constants, lifetimes and diffusion lengths, respectively. J_n, J_p are the electron and hole currents, while p_n^o and n_p^o are the equilibrium hole and electron concentrations in n-type and p-type material respectively. The boundary conditions are determined by the minority carrier concentration at the junction depletion edges and at the surfaces (i.e. the emitter and collector contact ends). In computing the device characteristics, it is assumed that the transistor is operating in the normal, active mode in a common emitter configuration, with a fixed V_{CE} and a forward bias V_{BE}. The boundary conditions at the space charge edges, or the junction law [22], are expressed as:

$$p - p_E^o \Big|_{x = -X_E} = p_E^o[\ \exp(\ \frac{qV_{BE}}{kT}\ ) - 1\ ] \quad (2.7)$$

$$n - n_B^o \Big|_{x = 0} = n_B^o[\ \exp(\ \frac{qV_{BE}}{kT}\ ) - 1\ ] \quad (2.8)$$

$$n - n_B^o \Big|_{x = X_B} = n_B^o[\ \exp(\ \frac{qV_{BC}}{kT}\ ) - 1\ ] \quad (2.9)$$

$$p - p_C^o \Big|_{x = -X_C} = p_C^o[\ \exp(\ \frac{qV_{BC}}{kT}\ ) - 1\ ] \quad (2.10)$$

while the surface boundary conditions are given as:

$$D_E \frac{dp}{dx} \Big|_{x = -W_E - X_E} = s_F(\ p - p_E^o\ ) \quad (2.11)$$

$$p - p_C^o \Big|_{x = W_C + X_C} = 0 \quad (2.12)$$

where p_E^o, n_B^o and p_C^o are the equilibrium minority carrier concentrations in the emitter, base and collector respectively. V_{BC} is the base-collector bias, k is Boltzmann's constant, T the room temperature, D_E the emitter minority carrier diffusion constant, and s_F is the surface recombination velocity at the emitter contact. It is assumed that the collector end has an ohmic contact, therefore the surface recombination velocity there is infinite.

The various current components in the transistor are as shown in Figure 2.1. The electron current densities at the two neutral edges are denoted by $J_n(0)$ and $J_n(X_B)$. The hole

current density injected into the emitter from the base is represented by $J_p(-X_E)$, while the collector hole leakage current density is indicated by $J_p(X_C)$. These current components are calculated by imposing the boundary conditions (2.7)-(2.12) on the general current density expressions (2.5)-(2.6). The results are as follows:

$$J_p(-X_E) = \frac{qD_E p_E^o}{L_E} .\{ \exp(\frac{qV_{BE}}{kT}) - 1 \}$$
$$.\{ - \frac{s_F L_E}{D_E} .[1 + \exp(\frac{2.W_E}{L_E})]$$
$$+ [\exp(\frac{2.W_E}{L_E}) - 1] \}$$
$$.\{ \frac{s_F L_E}{D_E} .[1 - \exp(\frac{2.W_E}{L_E})]$$
$$+ [\exp(\frac{2.W_E}{L_E}) + 1] \}^{-1} \qquad (2.13)$$

$$J_n(0) = \frac{qD_B n_B^o}{L_B} \{ \exp(\frac{2.W_B}{L_B}) - 1 \}^{-1}$$
$$.\{ [\exp(\frac{qV_{BE}}{kT}) - 1].[\exp(\frac{2.W_B}{L_B}) + 1]$$
$$- 2.\exp(\frac{W_B}{L_B}).[\exp(\frac{qV_{BC}}{kT}) - 1] \}$$
$$(2.14)$$

$$J_n(X_B) = \frac{qD_B n_B^o}{L_B} \{ \exp(\frac{2.W_B}{L_B}) - 1 \}^{-1}$$

$$.\{ -[\exp(\frac{qV_{BC}}{kT}) -1].[\exp(\frac{2.W_B}{L_B}) +1]$$

$$+ \ 2.\exp(\frac{W_B}{L_B}).[\exp(\frac{qV_{BE}}{kT}) - 1] \}$$

(2.15)

$$J_p(X_C) = \frac{qD_C p_C^o}{L_C} [\exp(\frac{qV_{BC}}{kT}) - 1] \qquad (2.16)$$

In the above equations D_B, D_C are the minority carrier diffusion constants in the base, collector; and L_E, L_B, L_C are the minority carrier diffusion lengths in the emitter, base, collector respectively.

The current components due to the generation and recombination of carriers in the junction space charge regions are given below. The recombination current in the forward biased emitter-base junction, J_{REC}, is expressed by Choo's equations for an asymmetrically doped step junction, namely [23]:

$$J_{REC} = \frac{qn_i W_{BE}}{\sqrt{(\tau_B . \tau_E)}} \cdot \frac{2.\sinh(\frac{qV_{BE}}{2.kT})}{q/kT.(V_{biE} - V_{BE})} . f(b)$$

(2.17)

where

$$f(b) = \frac{1}{\sqrt{(\ 1 - b^2\ )}} \cdot \tan^{-1}\left[\frac{\kappa}{\gamma} \sqrt{(\ 1 - b^2\ )} \right]$$

$$\text{for } b < 1 \qquad (2.18a)$$

$$f(b) = \frac{1}{\sqrt{(\ b^2 - 1\ )}} \cdot \tanh^{-1}\left[\frac{\kappa}{\gamma} \sqrt{(\ b^2 - 1\ )} \right]$$

$$\text{for } b > 1 \qquad (2.18b)$$

$$f(b) = \frac{\kappa}{\gamma} \qquad \text{for } b = 1 \qquad (2.18c)$$

and

$$b = \exp\left(- \frac{qV_{BE}}{kT} \right) \cdot \cosh\left[\frac{E_t - E_i}{kT} + \frac{1}{2} \ln\left(\frac{\tau_E}{\tau_B} \right) \right] \qquad (2.19)$$

$$\kappa = 2.\sinh\left[\frac{q(\ V_{biE} - V_{BE}\ )}{k.T} \right] \qquad (2.20)$$

$$\gamma = \sqrt{\left(\frac{\tau_B N_B}{\tau_E N_E} \right)} + \sqrt{\left(\frac{\tau_E N_E}{\tau_B N_B} \right)} + 2b.\cosh\left[\frac{q(\ V_{biE} - V_{BE}\ )}{k.T} \right] \qquad (2.21)$$

$$V_{biE} = \frac{k.T}{q} \cdot \ln\left[\frac{N_E N_B}{n_i^2} \right] \qquad (2.22)$$

$$W_{BE} = \sqrt{\left(\frac{2\epsilon V_{biE}}{q} \cdot \frac{N_E+N_B}{N_E.N_B} \right)} \qquad (2.23)$$

The generation current in the reverse-biased collector-base junction, J_{GEN}, is given by the general Sah-Noyce-Shockley equation [24]:

$$J_{GEN} = \frac{qn_i W_{BC}}{2.\sqrt{(\tau_B.\tau_C)}} \cdot \cosh\left[\frac{E_t-E_i}{kT} + \frac{1}{2} .\ln\left(\frac{\tau_C}{\tau_B} \right) \right]^{-1} \qquad (2.24)$$

where

$$W_{BC} = \sqrt{\left(\frac{2\epsilon V_{biC}}{q} \cdot \frac{N_C+N_B}{N_C.N_B} \right)} \qquad (2.25)$$

$$V_{biC} = \frac{k.T}{q} \cdot \ln\left[\frac{N_C N_B}{n_i^2} \right] \qquad (2.26)$$

V_{biE} and V_{biC} are the built-in voltages at the base-emitter and base-collector junctions while W_{BE} and W_{BC} are the emitter and collector depletion widths, respectively. N_E, N_B, N_C are the doping levels in the emitter, base and collector respectively. n_i, ϵ and E_i are, respectively, the intrinsic carrier concentration, permittivity, and intrinsic Fermi level in GaAs, while E_t is the energy level of the recombination centers present in the material.

In using the expressions for J_{REC} and J_{GEN}, it is assumed that there are single-level, uniformly distributed recombination-generation centers located at or near the

intrinsic Fermi level, therefore E_t is approximately equal to E_i. It is further assumed that the recombination-generation mechanism involved is of the Shockley-Read-Hall type. This assumption is supported by minority carrier diffusion length studies in GaAs by various authors. Sekela et al. [25] showed in their studies of hole diffusion length in n-type GaAs that the largest L_p measured is about one third that of the theoretical value predicted by Ryan and Eberhardt [26] for radiative recombination, which implies that the hole lifetime due to indirect recombination is typically an order of magnitude lower than that due to direct radiative recombination. The studies on electron diffusion length in p-type GaAs by Casey et al. [27,28] also indicated that the electron lifetime is dominated by nonradiative recombination for hole concentrations less than $1x10^{18}$ cm^{-3}. This insignificant contribution of radiative recombination to the total recombination mechanism can be attributed to the presence of a large number of recombination centers and defects in GaAs [29], despite the fact that GaAs is a direct bandgap semiconductor. The Shockley-Read-Hall recombination is assumed to be the dominant component of the indirect recombination mechanism since it is believed that Auger recombination is important in GaAs only at very high doping densities (greater than 10^{19} cm^{-3}) [30].

The terminal current densities are calculated by summing up the current components in equations

(2.13-2.17,2.24). The total base current density is given by:

$$J_B = J_p(-X_E) + J_n(0) - J_n(X_B) - J_p(X_C) + J_{REC} - J_{GEN} \quad (2.27)$$

And the collector current density is given as:

$$J_C = J_n(X_B) + J_p(X_C) + J_{GEN} \quad (2.28)$$

The static current gain, β or h_{fe}, is expressed as the ratio of the collector and base current densities:

$$\beta = \frac{J_C}{J_B} \quad (2.29)$$

2.3 THE MODEL PARAMETERS

In the model, the thermal equilibrium carrier concentrations are computed using Fermi-Dirac statistics to account for carrier degeneracy. The densities of electrons and holes in the conduction and valence bands are given by the conventional forms:

$$n(cm^{-3}) = N_C \cdot F_{1/2}(\eta) \quad (2.30)$$

$$p(cm^{-3}) = N_V \cdot F_{1/2}(\xi) \quad (2.31)$$

where

$$\eta = \frac{E_f - E_g}{kT} \tag{2.32}$$

and

$$\xi = \frac{-E_f}{kT} \tag{2.33}$$

In these equations, n, p are the electron and hole concentrations respectively, $F_{1/2}(x)$ is the Fermi-Dirac Integral of order 1/2, approximated by accurate, low order polynomials [31], E_f is the Fermi energy, and E_g is the width of the forbidden energy bandgap in eV. The zero reference for the energy levels is taken at the valence band edge.

The effective densities of states, in the appropriate bands, are expressed as:

$$N_C(cm^{-3}) = 2.\left[\frac{2\pi m_e^* kT}{h^2}\right]^{3/2}. 10^{-6} \tag{2.34}$$

$$N_V(cm^{-3}) = 2.\left[\frac{2\pi m_h^* kT}{h^2}\right]^{3/2}. 10^{-6} \tag{2.35}$$

where h is Planck's constant. The effective mass of electrons, m_e^* in the conduction band system, is given by Blakemore [32] as an averaging function of the effective masses of electrons in the lowest conduction band minima, Γ_6, and the two higher energy valleys, L_6 and X_6. The non-parabolic effect of the lowest band is also included by an additional term in the expression for the Γ_6 mass

parameter:

$$m_e^* = \{ m_{co}^{3/2} . [1 - \frac{15\alpha kT}{4E_g} . \frac{F_{3/2}(\eta)}{F_{1/2}(\eta)}] + m_X^{3/2} . [\frac{\exp(\eta - \frac{\Delta\Gamma_X}{k.T})}{F_{1/2}(\eta)}] + m_L^{3/2} . [\frac{\exp(\eta - \frac{\Delta\Gamma_L}{k.T})}{F_{1/2}(\eta)}] \}^{2/3} \qquad (2.36)$$

The scalar effective mass of the Γ_6 band, m_{co} is equal to $0.0632m_0$; where m_0 is the free electron mass (9.1095×10^{-31} kg). The non-parabolic coefficient α is equal to -0.824. m_X, m_L are the effective masses of the two higher energy minima, which are assigned values of $0.55m_0$ and $0.85m_0$ respectively. $\Delta\Gamma_L$=0.284 eV, $\Delta\Gamma_X$=0.476 eV are the energy separations between the Γ-L and Γ-X bands. $F_{3/2}(x)$ the Fermi-Dirac Integral of order 3/2, comes from the k^4 term in the energy-wavevector relation of the Γ_6 band. This integral is computed using short series approximations [31]. For n-type, weakly-doped GaAs at room temperature, m_e^* can be approximated by the first term of equation (2.36), since the fractions of electrons in the L_6, X_6 bands are relatively small. However, for a heavily doped material such that $\eta \geq 0$, the contributions from the electron population in the two upper bands are non-negligible and lead to an increased electron effective mass.

The hole effective mass is also calculated from the detailed equation of the light hole and heavy hole bands in the valence band system [32]:

$$m_h^* = \{ m_h^{3/2} + m_L^{3/2} . [1 - \frac{15BkT}{4E_g} \frac{F_{3/2}(\xi)}{F_{1/2}(\xi)}] \}^{2/3} \quad (2.37)$$

where m_h, m_L are the heavy hole and light hole effective masses, taken as $0.5m_o$ and $0.088m_o$ respectively. The non-parabolic coefficient B of the light hole band is equal to -3.80.

To compute the carrier effective masses, and hence the carrier concentrations, the actual bandgap and the exact location of the Fermi level are required. At high doping levels, the energy bandgap is effectively reduced, due to the overlapping of impurity bands with the tail states of the conduction and valence band system. This bandgap narrowing effect can be related to the effective intrinsic carrier concentration such that [32,33]:

$$E_g(eV) = 1.42248 - \Delta E_g \quad (2.38)$$

and

$$\Delta E_g(eV) = kT . \ln[\frac{n_i^2}{n_{ie}^2}] \quad (2.39)$$

The value of the intrinsic carrier concentration n_i at room temperature has been determined by various experiments and

shown to vary from 1.8×10^{6} cm^{-3} to 3.0×10^{6} cm^{-3} [34]. It is taken as 2×10^{6} cm^{-3} in the model. The variation of the effective intrinsic carrier concentration n_{ie} with doping density is expressed by the empirical relations of Bailbe et al. [35], namely:

for n-type material,

$$n_{ie}(cm^{-3}) = 9\times10^{5} + 3.38\times10^{-3}.\sqrt{(N_D)} - 3.47\times10^{-5}.\ln\left[\frac{N_D}{10^{17}}\right] \qquad (2.40)$$

and for p-type material,

$$n_{ie}(cm^{-3}) = 9\times10^{5} + 3.38\times10^{-3}.\sqrt{(N_A)} - 6.72\times10^{-5}.\ln\left[\frac{N_A}{10^{17}}\right] \qquad (2.41)$$

The Fermi level is computed by achieving the charge neutrality condition, in which the total negative charges (electrons and ionized acceptors) are equal to the total positive charges (holes and ionized donors) :

$$n + N_A^{-} - (p + N_D^{+}) = 0 \qquad (2.42)$$

The number of ionized impurities, N_i is given by:

$$N_i(cm^{-3}) = \frac{N_t}{1 + g.\exp(\Delta)} \qquad (2.43)$$

where N_t is the total density of impurity dopant in cm^{-3}, g is the degeneracy factor (2 for acceptors, 4 for donors), and $\Delta = (E_f - E_g + E_A)/kT$ for donor states and $(E_A - E_f)/kT$ for acceptor states.

The impurity activation energy relative to the appropriate band is described by the empirical relation [36]:

$$E_A(eV) = E_A^o - A.N_t^{1/3} \qquad (2.44)$$

where E_A^o is the activation energy for infinite dilution. The coefficient A is taken as $1.9x10^{-8}$ cm.eV for n-type dopant [37], and $2.3x10^{-8}$ cm.eV for p-type dopant [38]. The $N_t^{1/3}$ dependence comes from the relation between the impurity atom spacing and concentration.

In the diffusion current calculations, minority carrier parameters such as diffusion constants and lifetimes are needed besides the equilibrium carrier concentrations. The electron and hole diffusion constants are expressed by the generalized Einstein relation, written as a rapidly converging series [39]:

$$D_n(cm^2sec^{-1}) = \mu_n \frac{k.T}{q} \left[1 + 0.35355 \left(\frac{n}{N_C}\right) - 9.9x10^{-3} \left(\frac{n}{N_C}\right)^2 + 4.45x10^{-4} \left(\frac{n}{N_C}\right)^3 \right] \qquad (2.45)$$

$$D_p(cm^2sec^{-1}) = \mu_p \frac{k.T}{q} \left[1 + 0.35355 \left(\frac{p}{N_V}\right) - 9.9x10^{-3} \left(\frac{p}{N_V}\right)^2 + 4.45x10^{-4} \left(\frac{p}{N_V}\right)^3 \right] \quad (2.46)$$

where μ_n, μ_p are the minority carrier mobilities for electrons and holes.

To model the carrier mobilities, data from Hall effect measurements for electron mobility in n-type GaAs [37,40-45], and hole mobility in p-type GaAs [38,40-41,46-49] are gathered and fitted with a fifth order least square polynomial against the majority carrier concentration:

$$\mu_H(cm^2V^{-1}sec^{-1}) = \sum_{i=0}^{5} A_i.x^i \quad (2.47)$$

where $x=Log_{10}(n/cm^{-3})$ for n-type material and $Log_{10}(p/cm^{-3})$ for p-type material. The coefficients A_i for both electron and hole Hall mobility are listed in Table 2.1. The experimental data for electrons and holes together with the fitted curve from equation (2.47) are plotted in Figures 2.2 and 2.3 respectively.

It is assumed that the values of Hall mobility have been measured under low magnetic field intensities so that the majority carrier drift mobility can be obtained by dividing the Hall mobility by the weak field Hall factor R_H:

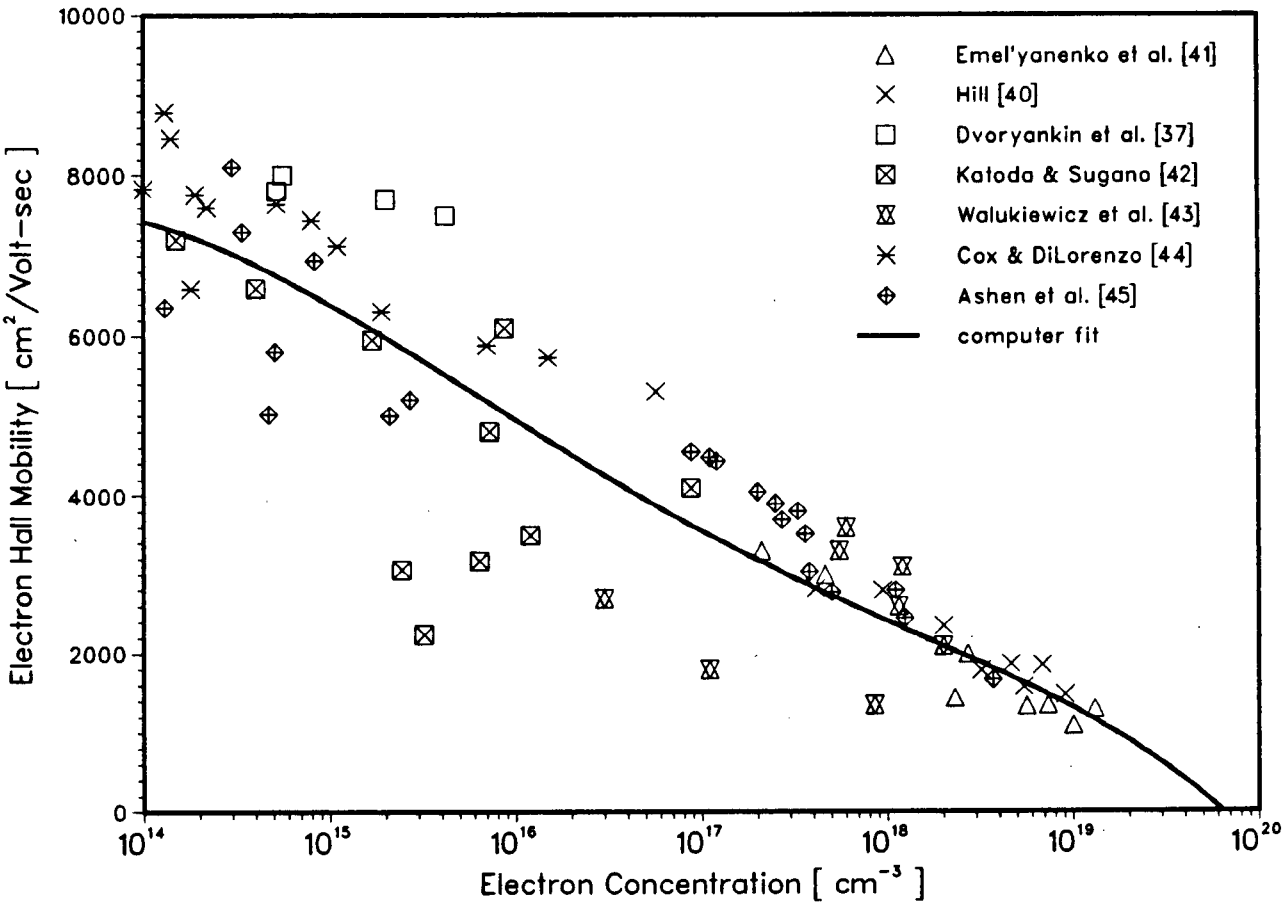

Fig. 2.2 Experimental data and best curve fit for the dependence of electron Hall mobility on majority carrier concentration.

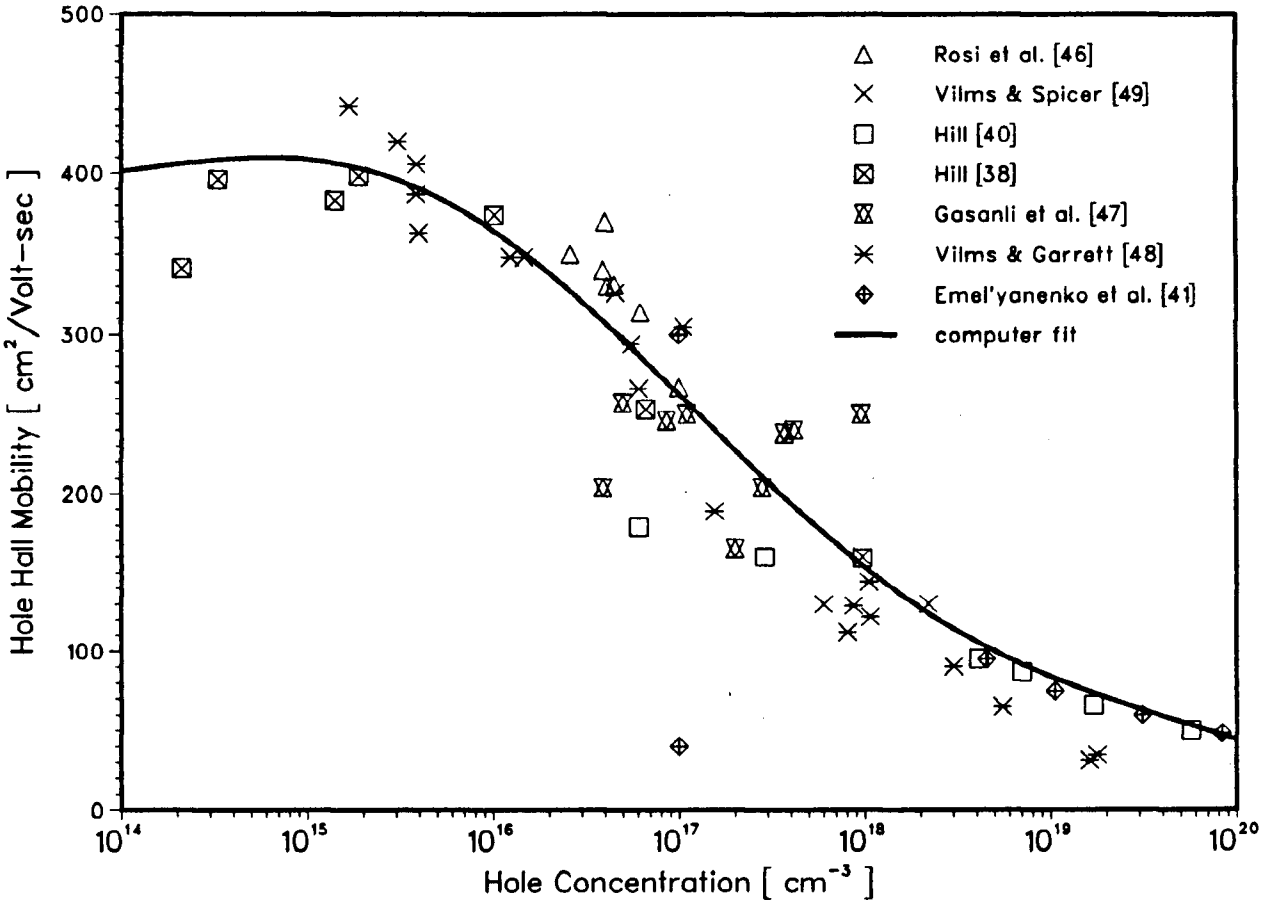

Fig. 2.3 Experimental data and best curve fit for the dependence of hole Hall mobility on majority carrier concentration.

$$\mu(cm^2V^{-1}sec^{-1}) = \frac{\mu_H}{R_H} \qquad (2.48)$$

where R_H is taken as 1.175 and 1.25 for electron and hole Hall mobility respectively [32].

For electrons, the ratio of minority carrier to majority carrier mobility is described by:

$$\mu_n^p(cm^2V^{-1}sec^{-1}) = f(n) \cdot \mu_n^n \qquad (2.49)$$

where μ_n^p, μ_n^n are the respective electron drift mobilities in p-type and n-type material. f(n) represents a 4th order polynomial fitted to the data of reference [50]:

$$f(n) = 684.327 - 168.175y + 15.497y^2 - 0.633y^3 + 0.009y^4 \qquad (2.50)$$

where $y=Log_{10}(n/cm^{-3})$. The dependence of f(n) on electron concentration is plotted in Figure 2.4. For holes, a similar expression relating the majority carrier to the minority carrier mobility does not exist. Therefore the mobility ratio for holes is assumed to be unity.

Curve fittings are also performed on data for electron [49,51-54] and hole [51,53-58] minority carrier lifetimes. These data are plotted in Figures 2.5 and 2.6. The fitted curves are of the form:

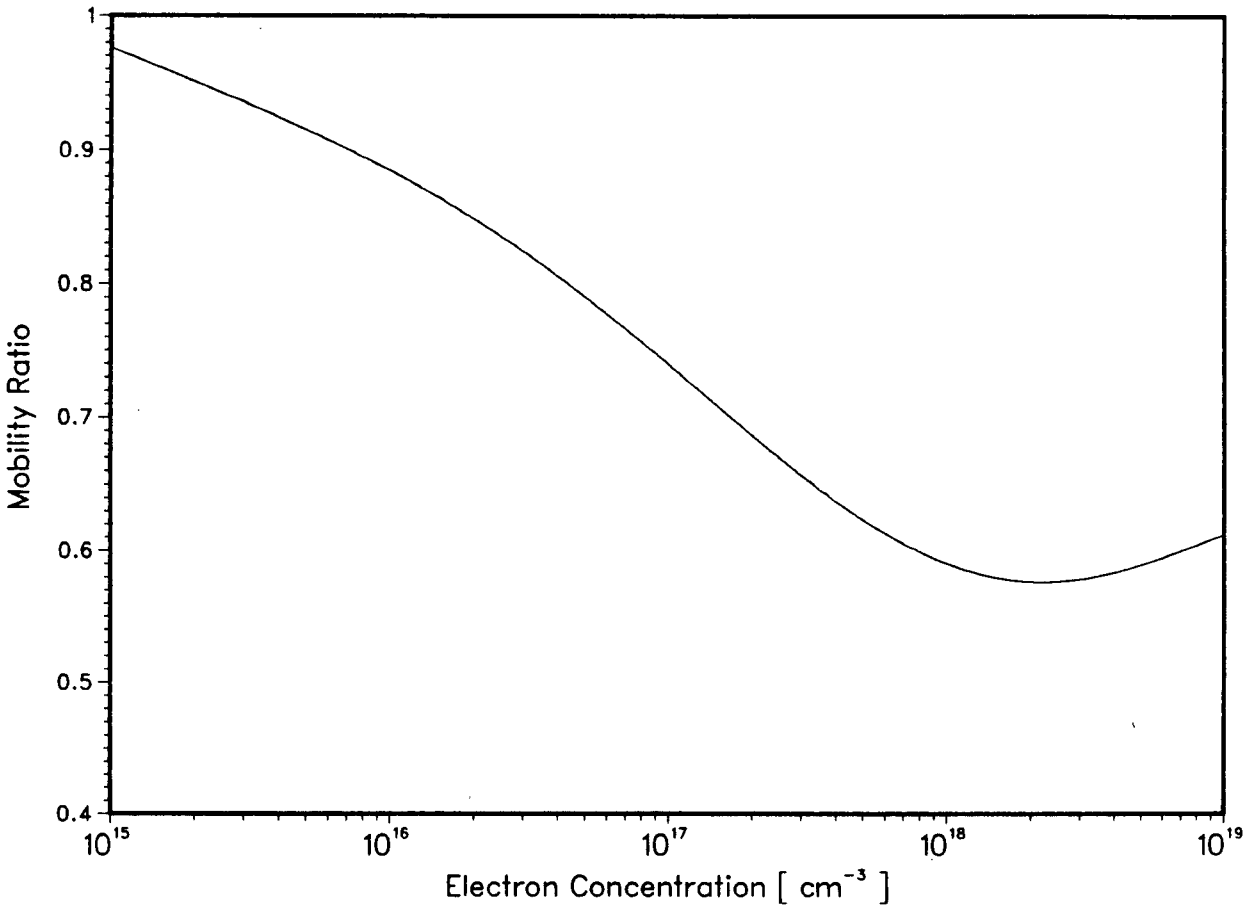

Fig. 2.4 Ratio of electron mobility in p-type GaAs, μ_n^p, to the electron mobility in n-type GaAs, μ_n^n, as a function of electron concentration.

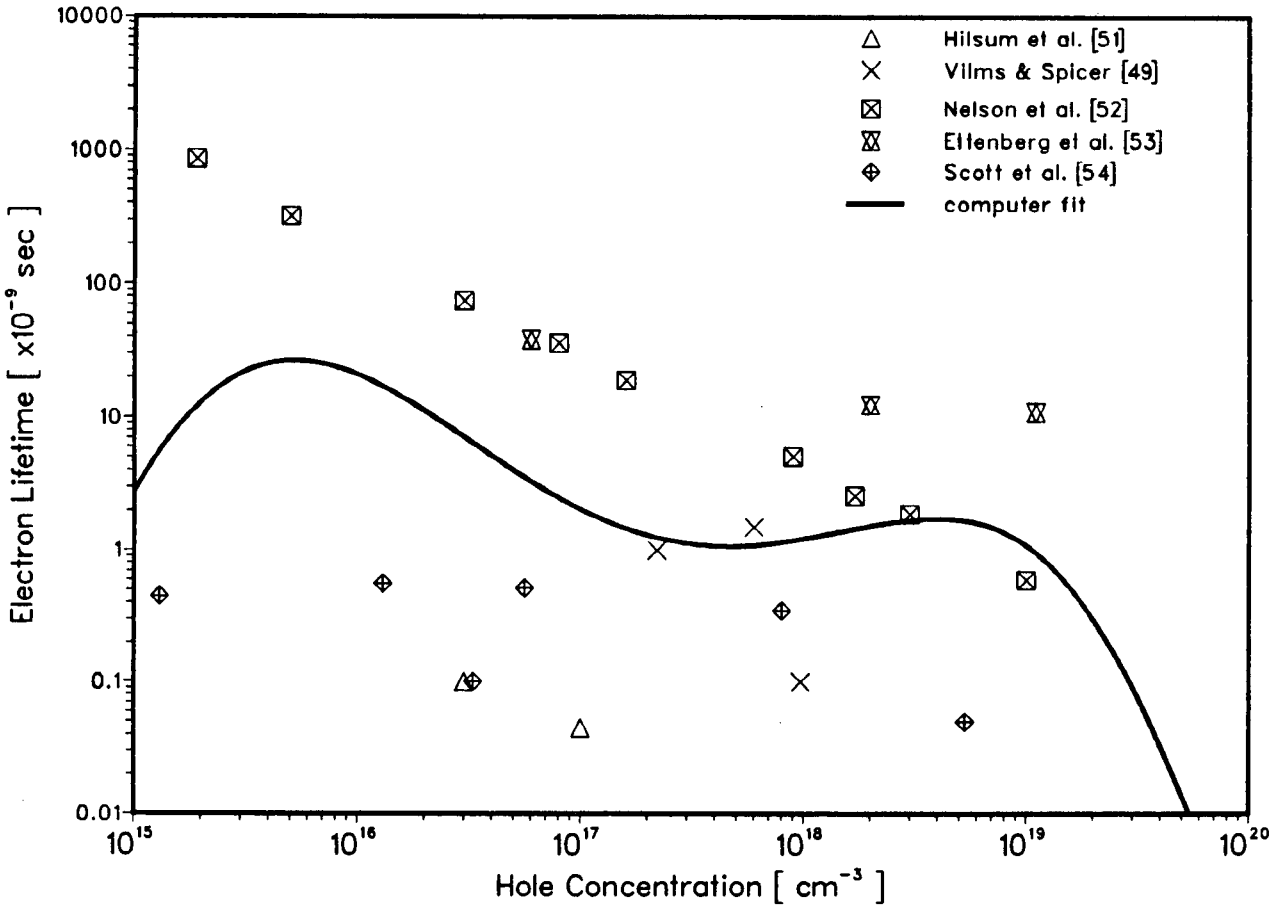

Fig. 2.5 Experimental data and best curve fit for the dependence of electron lifetime on hole concentration.

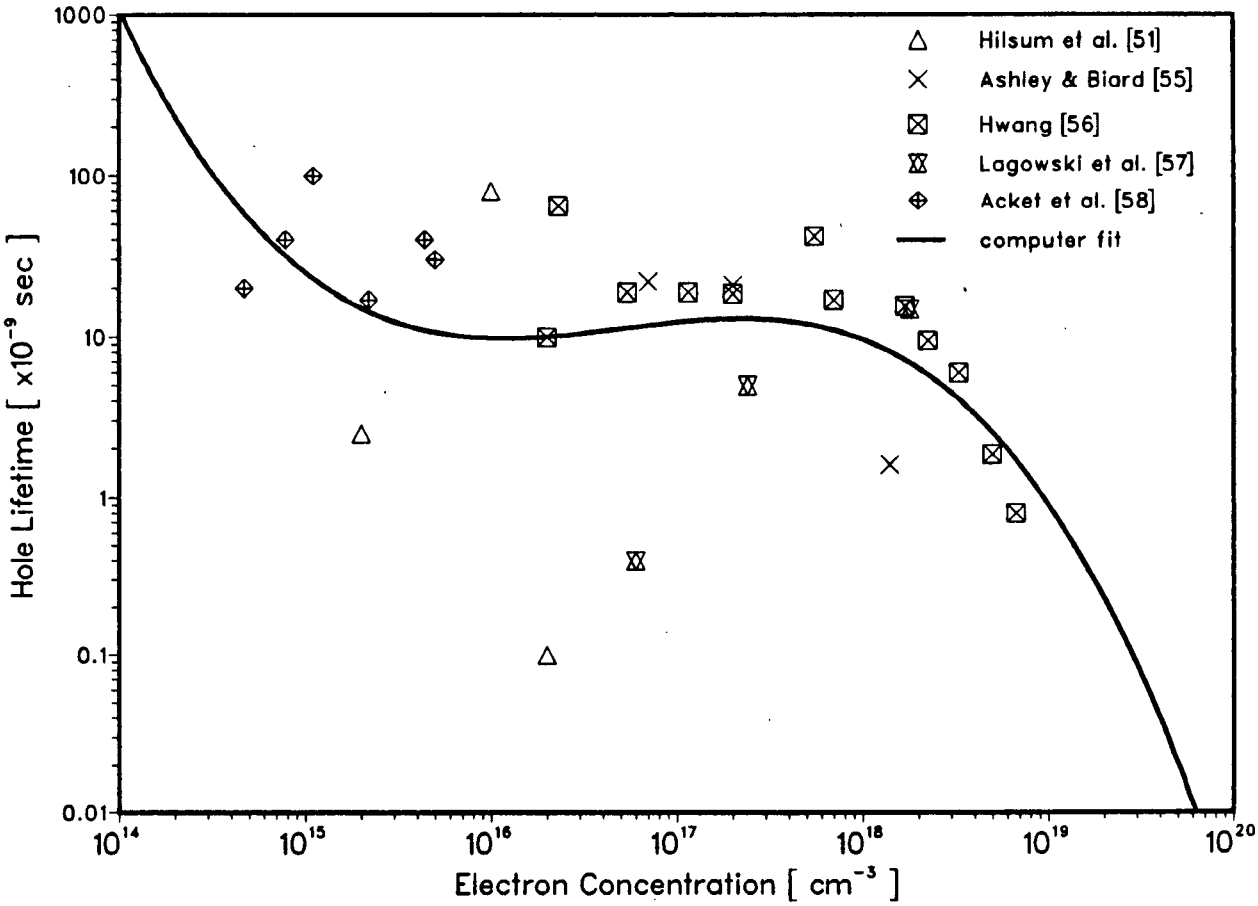

Fig. 2.6 Experimental data and best curve fit for the dependence of hole lifetime on electron concentration.

$$\mathrm{Log}_{10}(\tau/\mathrm{sec}) = \sum_{i=0}^{m} B_i . x^i \qquad (2.51)$$

where τ denotes the minority carrier lifetime. In this equation, $x=\mathrm{Log}_{10}(p/cm^{-3})$, m=5 for electron lifetime τ_n, and $x=\mathrm{Log}_{10}(n/cm^{-3})$, m=3 for hole lifetime τ_p. The coefficients B_i are given in Table 2.2.

To complete the set of parameters needed in the model calculations, the relative permittivity of GaAs is chosen as 13.1. The emitter surface recombination velocity is taken as $2x10^6$ cm^{-3} [57] except when it is specified as an input parameter.

2.4 THE SOLUTION PROCEDURE

To specify the model completely, input parameters such as semiconductor layer thicknesses and widths, and the bias voltages are required. These parameters are chosen for an ideal, uniformly doped bipolar transistor operating in the common emitter configuration, with profile and widths similar to that of the device reported in reference [17]. The input data are listed in Table 2.3. In the common emitter mode, the bipolar transistor is normally biased by a constant base current source. In this case, a constant voltage source, V_{BE} is used due to the ease of its implementation in the model. By doing so, it is assumed there is no temperature variation, so that the exponential

	Electron Hall Mobility ($cm^2V^{-1}sec^{-1}$)	Hole Hall Mobility ($cm^2V^{-1}sec^{-1}$)
A_0	0.053	502511.268
A_1	-69783.160	-156107.000
A_2	17348.328	19205.600
A_3	-1579.599	-1168.926
A_4	63.036	35.209
A_5	-0.935	-0.420

Table 2.1 Coefficients for μ_H in equation (2.47).

	$Log_{10}(\tau_n/sec)$	$Log_{10}(\tau_p/sec)$
B_0	$-7.632X10^{-6}$	545.075
B_1	-678.572	-99.574
B_2	157.935	5.967
B_3	-13.738	-0.119
B_4	0.531	
B_5	-0.007	

Table 2.2 Coefficients for minority carrier lifetimes in equation (2.51).

N_E	Emitter doping density	$1x10^{18}$ cm^{-3}
N_B	Base doping density	$1x10^{17}$ cm^{-3}
N_C	Collector doping density	$1x10^{16}$ cm^{-3}
W_E	Emitter layer thickness	0.25 μm
W_B	Base layer thickness	0.40 μm
W_C	Collector layer thickness	2.00 μm
s_F	Emitter surface recombination velocity	$2x10^6$ cm sec^{-1}
V_{CE}	Emitter-collector reverse bias voltage	5.0 V
V_{BE}	Emitter-base forward bias voltage	0.6 - 1.30 V

Table 2.3 Input data used in the modeling program.

term involving qV_{BE}/kT, which determines the base current, is the same for a given V_{BE}.

The flow chart for the modeling program is given in Figure 2.7. In this analytical analysis, the effect of changes in the widths, doping densities and minority carrier lifetimes of the emitter and base regions, the collector doping density and the emitter surface recombination velocity are examined by computing the variation of the DC gain versus collector current density. The input and output characteristics are also determined.

The solution procedure is as follows:

(1) Specify the device parameters and operating conditions.

(2) Read in the required sensitivity parameter.

(3) Calculate the activation energy and bandgap of the emitter region according to equations (2.38)-(2.41), (2.44).

(4) Compute the Fermi energy, the effective masses, densities of states and the carrier concentrations by solving the non-linear equation (2.42) using the subroutine ZERO.

(5) determine the minority carrier parameters: diffusion constants, mobilities and lifetimes according to equations (2.45)-(2.51).

(6) Repeat steps (3)-(5) for the base and collector regions.

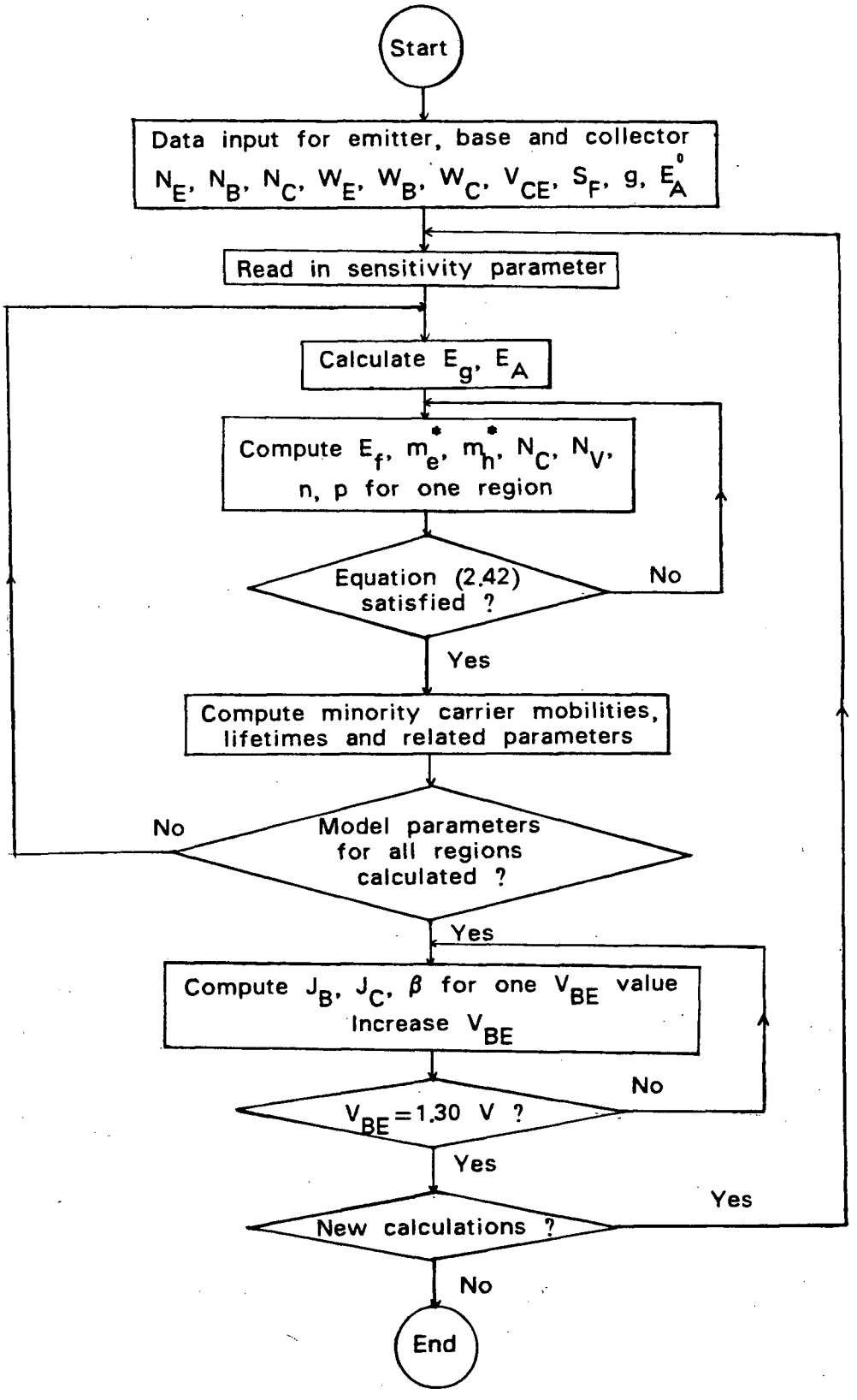

Fig. 2.7 Flow chart for the solution procedure of the analytical model.

(7) Calculate the base, collector current densities and DC gain using equations (2.13)-(2.17), (2.24), (2.27)-(2.29) for an initial V_{BE}.

(8) Increase V_{BE} and repeat step (7) until the final V_{BE} is reached. The program execution stops when all the sensitivity parameters have been read, otherwise steps (2)-(8) are repeated.

The same procedure is used to compute the device output characteristics, except the bias voltage is now V_{CE} and the calculations are computed for a fixed V_{BE}.

In the subroutine ZERO, the solution of a non-linear equation is obtained by a combination of the bisection and secant methods [59]. Let the net charge function in equation (2.42) be F(x). An initial interval [B,C] is then chosen such that $F(B).F(C) \leq 0$. If F(B) is not equal to zero, an iteration is performed to find new values of B and C by shrinking [B,C], subject to the condition $|F(B)| \leq |F(C)|$. This iteration stops when the criterion $|B-C| \leq 2$(relative error.$|B|$ + absolute error) is reached. B is then the required solution. The absolute and initial relative error is chosen to be 1×10^{-6} in the program. The absolute error is needed in the event that the solution is 0. The modelling program is listed in Appendix A.

2.5 RESULTS AND DISCUSSION

To demonstrate the working of the analytical model, the transistor output characteristics are given in Figure 2.8. The curves are plotted for values of V_{BE} ranging from 1.10 V to 1.22 V as indicated. The input characteristics and the J_C - V_{BE} relationship are presented in Figure 2.9. As seen from this figure, in the low current range, J_B shows a voltage dependence of $(qV_{BE})/(nkT)$, where the ideality factor n = 1.89. This value is close to the theoretical value of 2 which would indicate that the base current density is dominated by J_{REC}, the space charge recombination current, see equation (2.17). As V_{BE} increases, J_{REC} becomes relatively less important, and the value of n is approximately equal to one, indicating the dominant component in the base current is that of the injected current. For the collector current density J_C, the ideality factor is 1.014 throughout the current range. This shows that J_C is predominantly $J_n(X_B)$, the injected electron current from the emitter which diffuses to the base-collector junction edge. This is as expected since the generation current in the reverse-biased junction, J_{GEN}, and the collector hole leakage current $J_p(X_C)$ are generally small when compared to the diffusion current.

To study the effects of base parameter variation on the transistor performance, plots of dc gain versus the collector current density using base lifetime and basewidth as parameters are shown in Figures 2.10 and 2.11. The

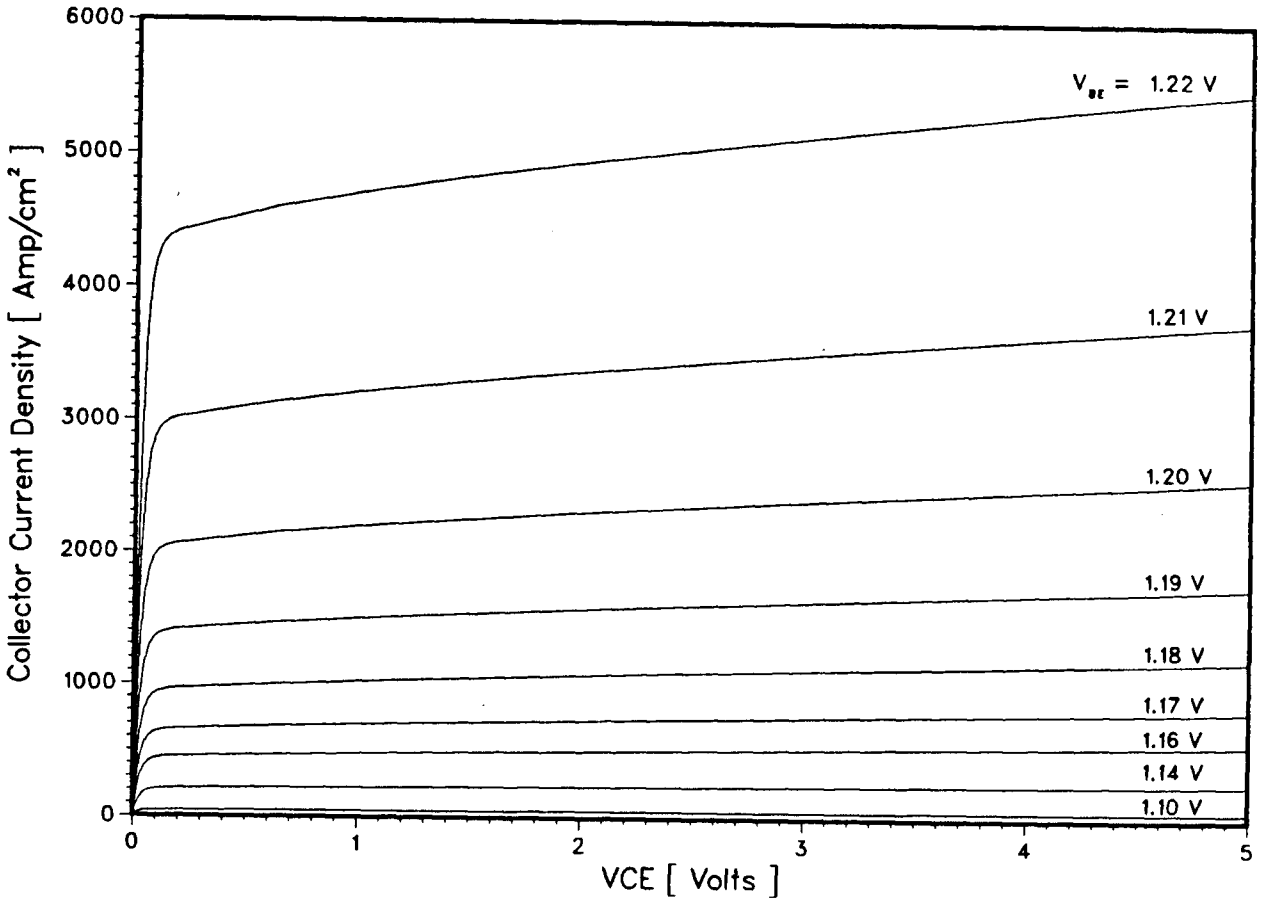

Fig. 2.8 Collector current density as a function of emitter-collector voltage with the base-emitter voltage as a parameter

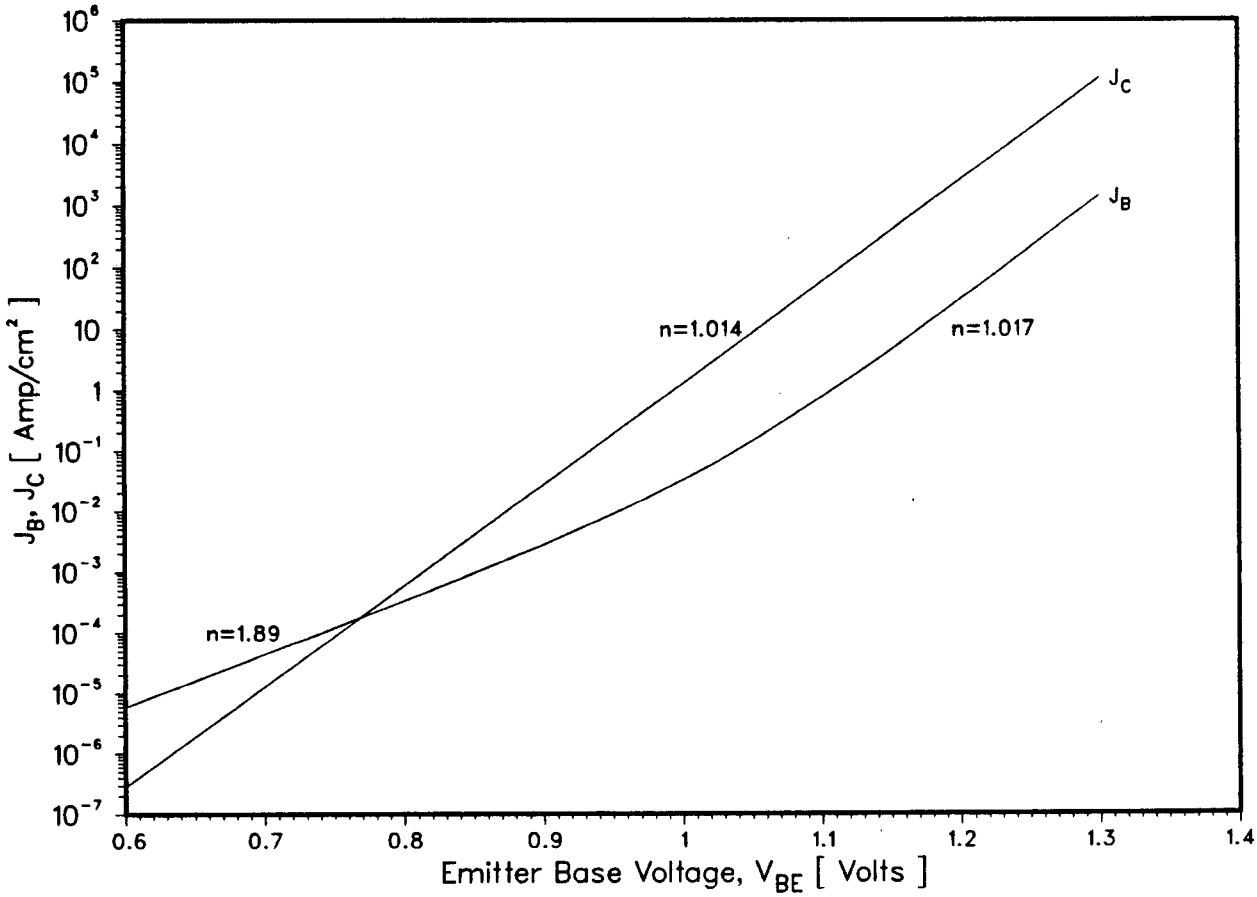

Fig. 2.9 Plot of base current density, collector current density versus base-emitter voltage. n is the ideality factor.

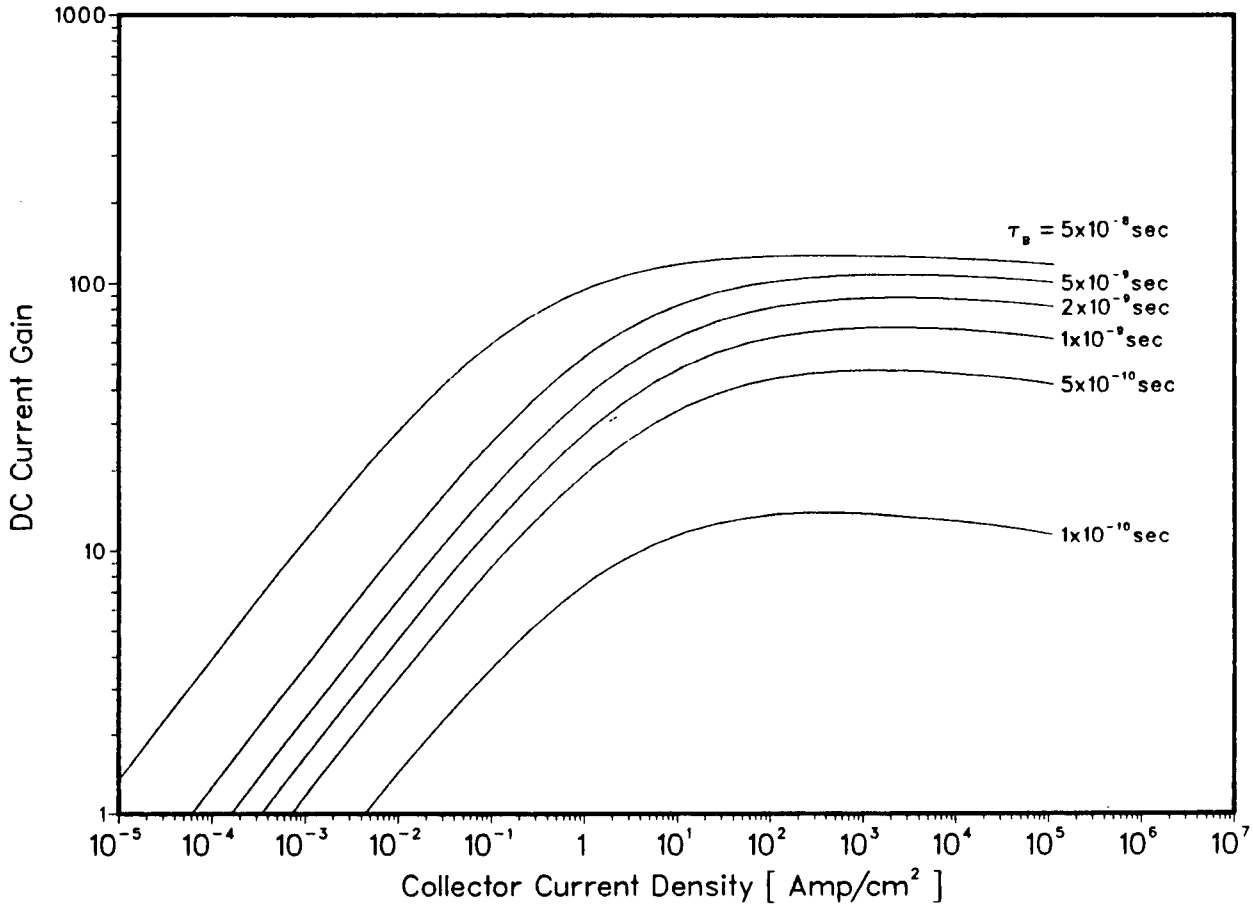

Fig. 2.10 The effect of electron lifetime in the base on gain, as predicted by the analytical model using the parameters listed in Table 2.3.

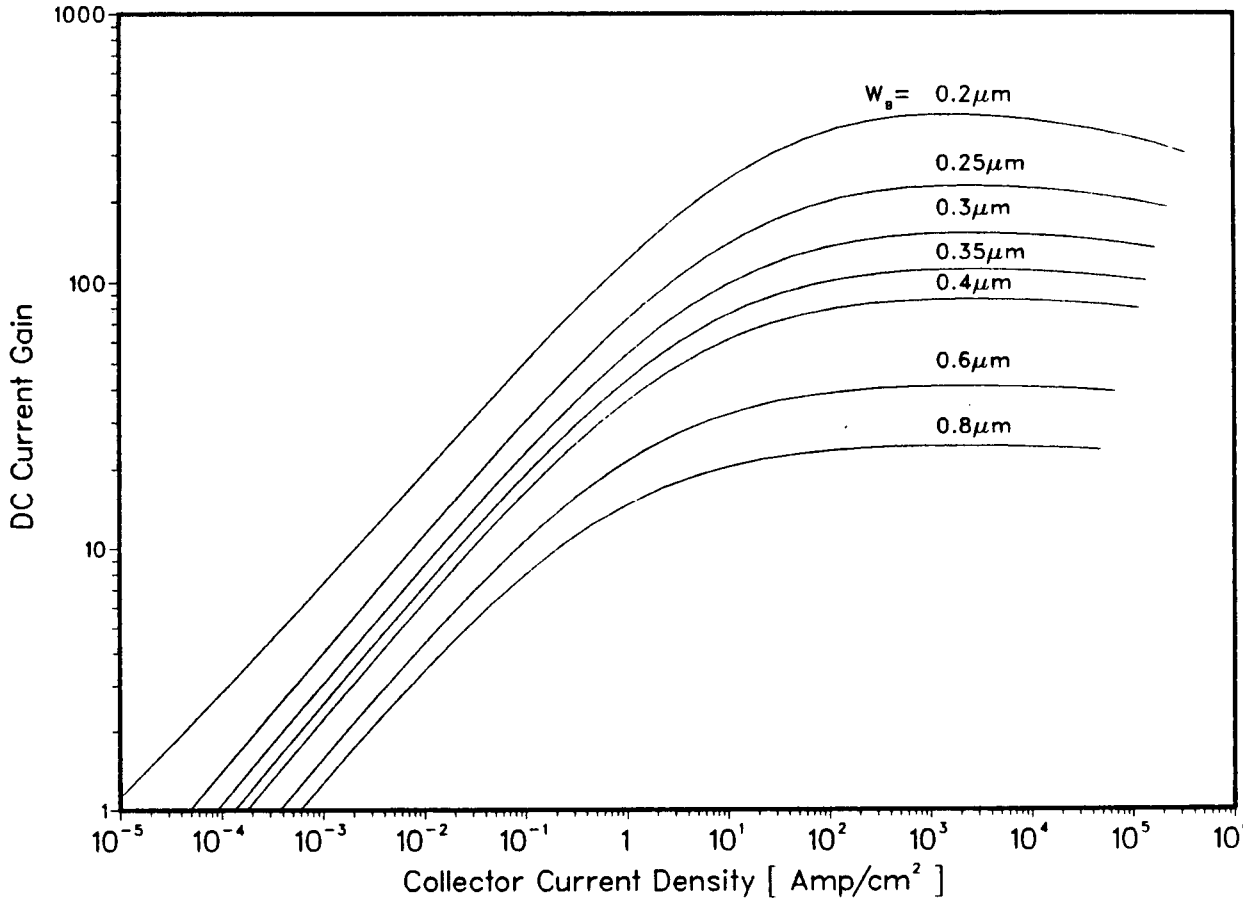

Fig. 2.11 The effect of basewidth on gain, as predicted by the analytical model using the parameters [other than W_B] listed in Table 2.3.

electron lifetime in p-type GaAs is known to be extremely short. Such a low minority carrier lifetime in the base region of a npn bipolar transistor has a profound effect on the dc gain. Because of their shorter diffusion length, more injected electrons from the emitter will recombine with holes present in the neutral base. The increase in base recombination brings about a decrease of the collector current, while at the same time, causes an increase of the base current. This will result in a substantial reduction in the transistor gain. Yuan et al. [15] estimated an electron lifetime in the base of their GaAs homojunction bipolar transistor to be 10^{-10} sec and held this responsible for the low value of h_{fe} of 8 which they measured in their experimental device. From Figure 2.10, it can be observed that for such a low base lifetime, gains exceeding 20 cannot be attained with a basewidth of 0.4 μm. For a base doping density of 10^{17} cm^{-3}, the longest lifetime ever measured in GaAs is close to $5x10^{-8}$ sec, as seen in Figure 2.5. Even for this value of lifetime, the gain obtained is only in the neighbourhood of 100. In view of this, a further increase in transistor gain will demand a narrower basewidth. From Figure 2.11, for a basewidth variation of 0.8 μm to 0.2 μm, the maximum gain increases from 15 to about 400. Therefore, a transistor gain of around 500 would require a basewidth of less than 0.2 μm, which is narrower than that in any of the devices reported so far. For a device with good base properties, the base transport factor will be very close to

one. In fact, in this case, a combination of high base lifetime of $5x10^{-8}$ sec and a basewidth of 0.2 μm yields a base transport factor of 0.9999. For such a high value of base transport factor, the common emitter gain will then be limited by the emitter injection efficiency, which is greatly influenced by the emitter back-injected hole current, $J_p(-X_E)$.

If the base properties could be improved such that the gain is only limited by the emitter back-injected hole current, then the effect of lifetimes, widths, doping densities and surface recombination in the emitter would have to be examined. The influence of emitter lifetime on dc gain is shown in Figure 2.12. For low collector currents, the effect of τ_E is the same as that of τ_B, due to the dominance of carrier recombination in the emitter-base junction depletion region, as indicated by J_{REC} in equation (2.17). At higher currents, the change in maximum gain obtained is only from 50 to 90 as the lifetime varies from a value of 10^{-10} sec to 10^{-7} sec. This insensitivity of gain to the change in τ_E can be attributed to the lack of dependence of the emitter Gummel number on τ_E. For instance, as τ_E changes from 10^{-10} sec to 10^{-7} sec, the Gummel number only increases from $2.4x10^{12}$ sec cm^{-4} to $4.74x10^{12}$ sec cm^{-4} at a collector current density of $\simeq 1x10^{4}$ Amp cm^{-2}. In addition, the relative change in emitter and base widths also brings about the saturation of the gain increase. As V_{BE} increases, both W_E and W_B becomes larger, with

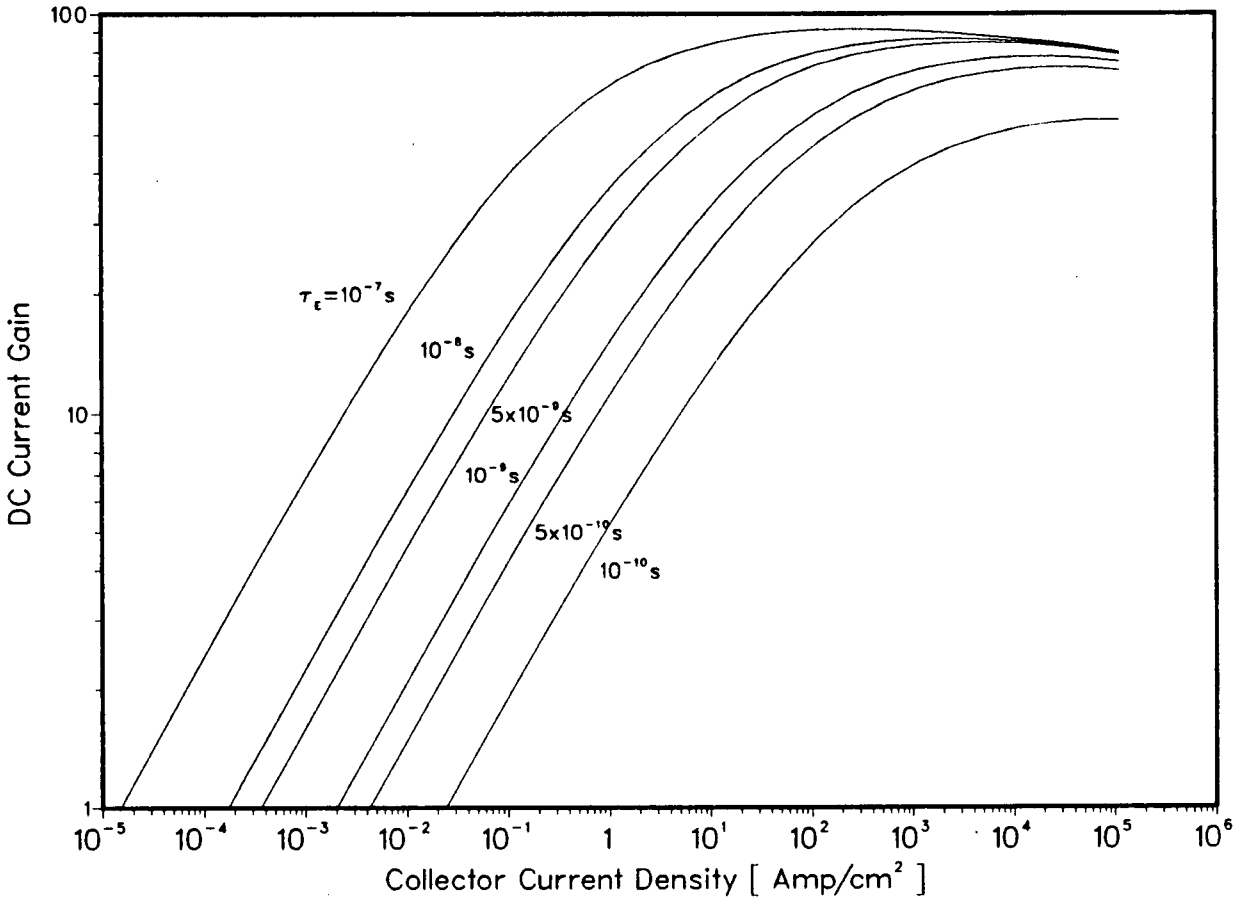

Fig. 2.12 The effect of hole lifetime in the emitter on gain, as predicted by the anlytical model using the parameters listed in Table 2.3.

the incremental change in W_B being comparatively more than for W_E due to the larger shrinkage in the base-collector depletion region. At a surface recombination velocity of $2x10^6$ cm/sec, the emitter contact is essentially an ohmic one. The increase in emitter width will reduce the back-injected hole current, as $J_p(X_E)$ varies as $\coth(W_E/L_E)$ for large s_F. As seen from Figure 2.13, the gain increases from about 40 to 120 for a variation of W_E from 0.1 μm to 0.5 μm. On the other hand, the larger basewidth also reduces the gain due to higher carrier recombination in the neutral base. The combined effect of the change in the widths of the base and emitter neutral regions is to reduce the amount of increase in gain.

The effect of surface recombination velocity on the transistor performance is shown in Figure 2.14. For the measured value of surface recombination velocity of $2x10^6$ cm/sec [57] at the emitter end, the transistor behaviour is effectively the same as for an ohmic contact with an emitter width of 0.25 μm. As a significant portion of the back injected hole current is due to the recombination of holes at the emitter surface, both a reduction in s_F and W_E would greatly improve the emitter injection efficiency. In fact, for an emitter width of 0.25 μm, a reduction of s_F to 100 cm/sec would increase the emitter injection efficiency to 0.9998. Further reduction in W_E could also improve the injection efficiency. However, such a low value of s_F has not yet been realised in GaAs

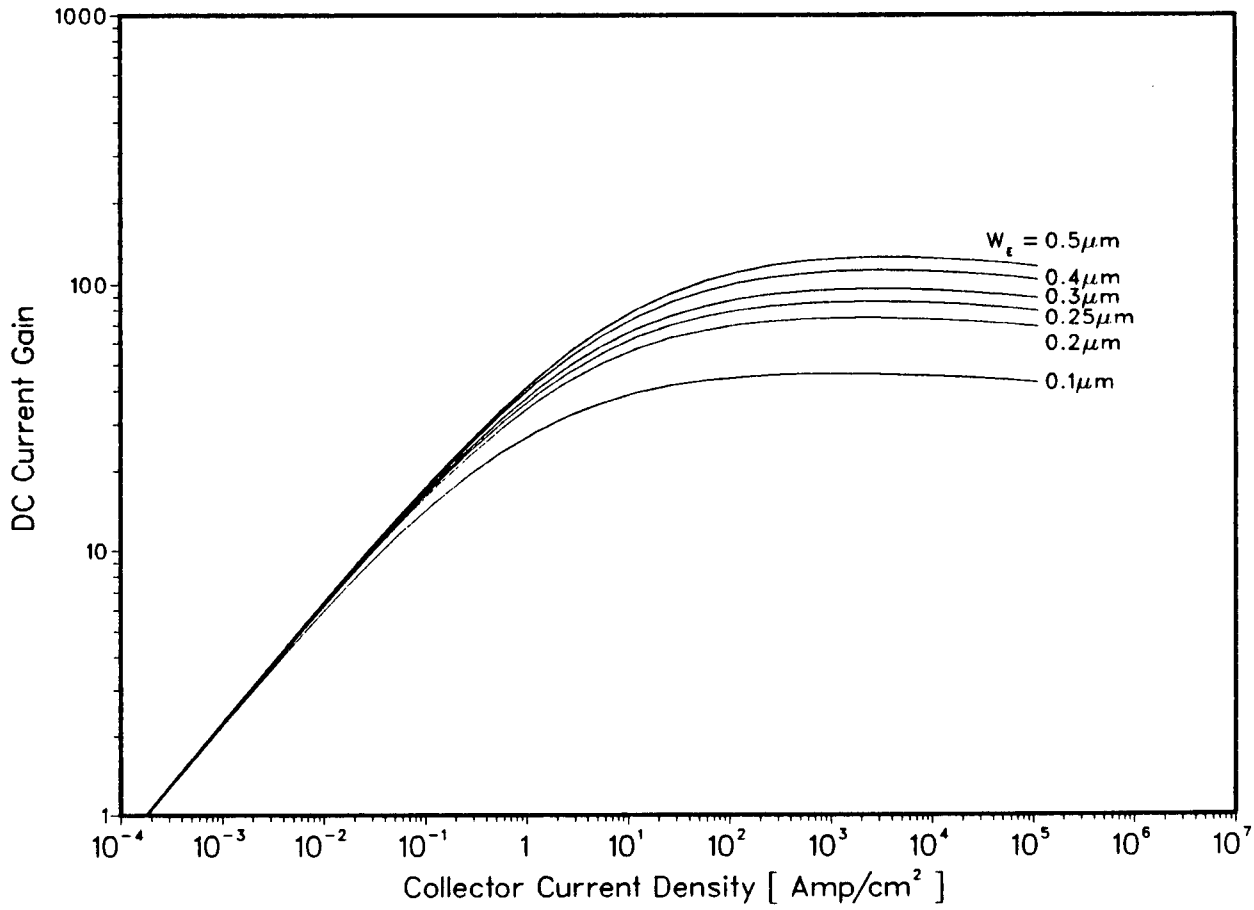

Fig. 2.13 The effect of emitter width on gain, as predicted by the analytical model using the parameters [other than W_E] listed in Table 2.3.

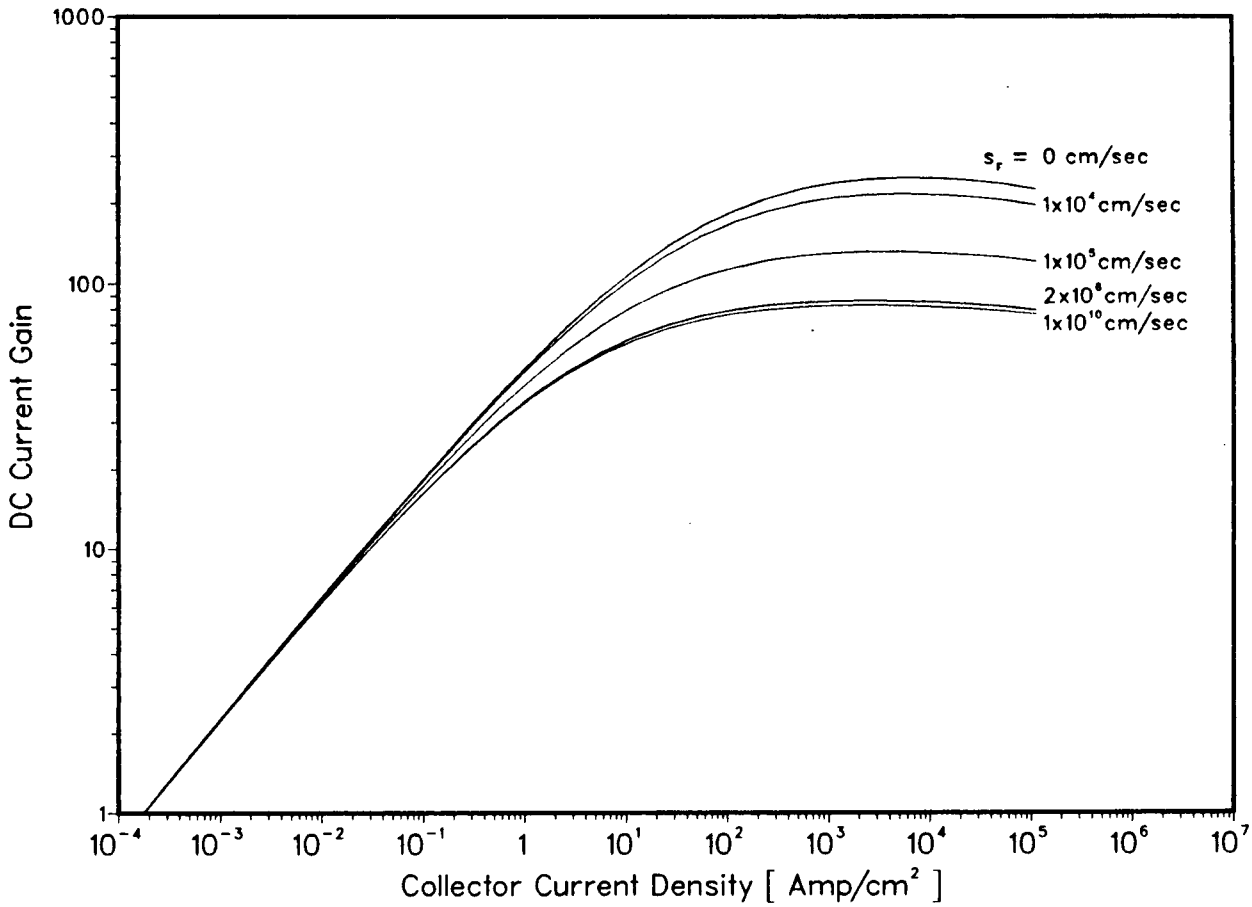

Fig. 2.14 The effect of surface recombination velocity on gain, as predicted by the analytical model using the parameters [other than s_F] listed in Table 2.3.

homojunction bipolar devices. To achieve values comparable to the best reported for Si devices (15 cm/sec for polysilicon contacts to silicon emitters [60]) would require improved passivation of the surface, or the use of a heterojunction emitter. Both these measures would serve to suppress the back injected hole current.

Another way of improving the emitter injection efficiency would be to use a more heavily doped emitter. However, as the emitter doping becomes very high, the effects of carrier degeneracy, and bandgap narrowing described by equations (2.38)-(2.41), cause a reduction of h_{fe}. The effect of emitter doping on gain is shown in Figure 2.15. In the low collector current range, heavy emitter doping results in a drop of h_{fe}. This is because the shrinkage of the energy bandgap in the emitter due to heavy doping results in an increased effective intrinsic carrier concentration, which in turn enhances the space charge recombination current, J_{REC}. As the base current density is dominated by J_{REC} in the low current range, a higher doping level in the emitter will increase J_B much more than J_C, thereby reducing β. In the higher collector current range, a β_{max} of about 270 is obtained for an emitter doping of $1x10^{19}$ cm^{-3} as compared to a β_{max} of about 90 for $N_E = 1x10^{18}$ cm^{-3}. The higher emitter doping reduces the number of holes present in the emitter, hence the emitter injection efficiency is greatly improved, due to the smaller back injected hole current $J_p(-X_E)$, as would be expected.

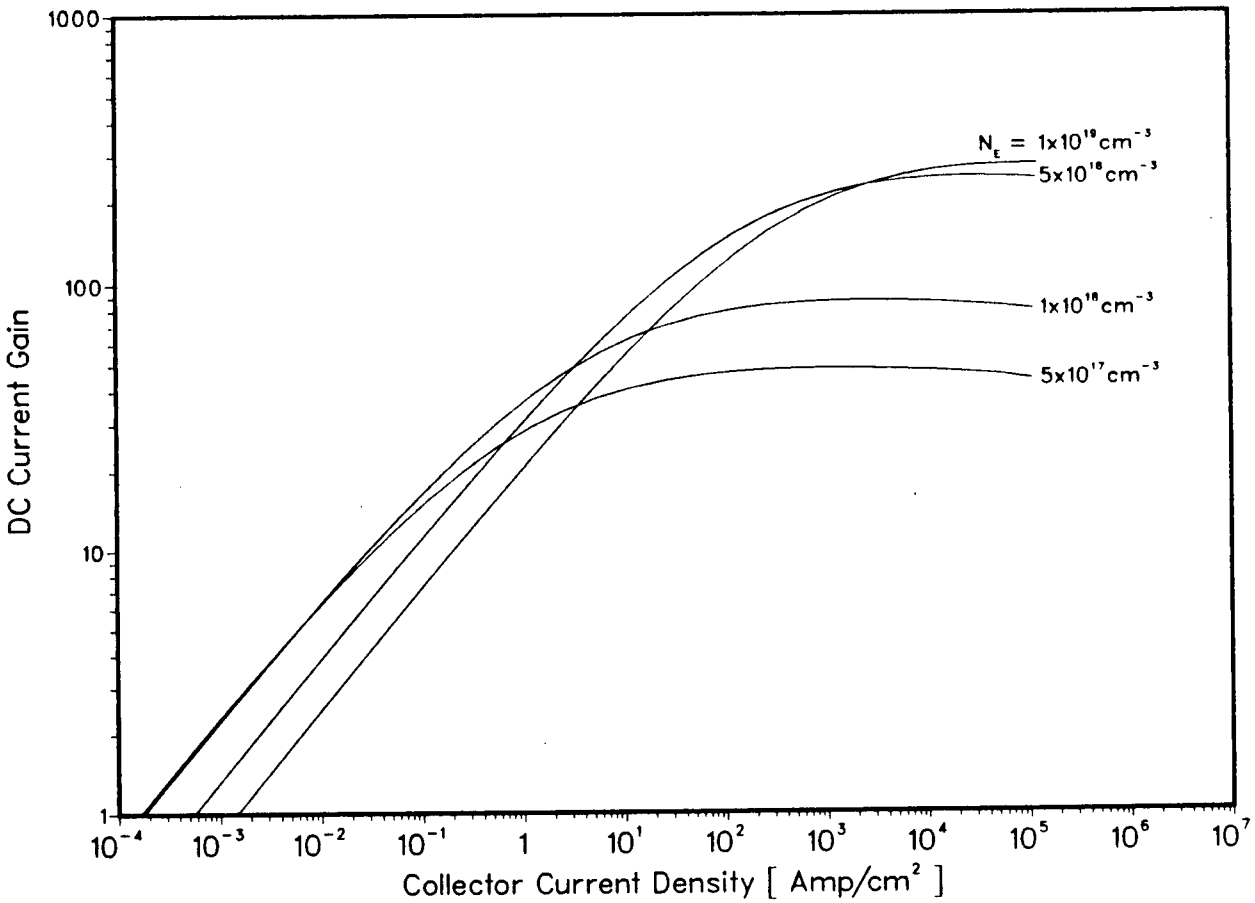

Fig. 2.15 The effect of emitter doping on gain, as predicted by the analytical model using the parameters [other than N_E] listed in Table 2.3.

For a heavily doped emitter, the bandgap narrowing should change the effective emitter doping density by a factor of (n_i^2/n_{ie}^2), where n_i and n_{ie} are the dilute and effective intrinsic carrier concentrations, respectively. However, in the cases under discussion, this correction is not significant and has little effect on the injection efficiency in the high current range.

The effect of collector doping on β is shown in Figure 2.16. The higher collector doping has the same result as would be achieved by effectively reducing the neutral basewidth. As the collector doping is increased, for a given base-collector reverse bias, most of the depletion region in the base-collector junction is extended into the base, resulting in a smaller neutral base. For instance, at a reverse bias V_{BC} of 4 Volts, the neutral basewidth is 0.322 μm for $N_C = 10^{14}$ cm^{-3}, and 0.06 μm for a collector doping of $8x10^{17}$ cm^{-3}. Therefore, it would be expected that β_{max} will be greater for higher collector doping densities. This is borne out by the results shown in Figure 2.16.

The model results for the devices studied by Tan and Milnes [5] are shown in Figure 2.17. Their devices were representative of transistors fabricated by MBE. This should lead to uniformly doped regions which are appropriate for analysing by the present model. The model predicts a maximum gain of 400, which is in good agreement with the values of "some hundred" estimated by the authors in Reference [5]. The simulation results for the devices of Bailbe et al.

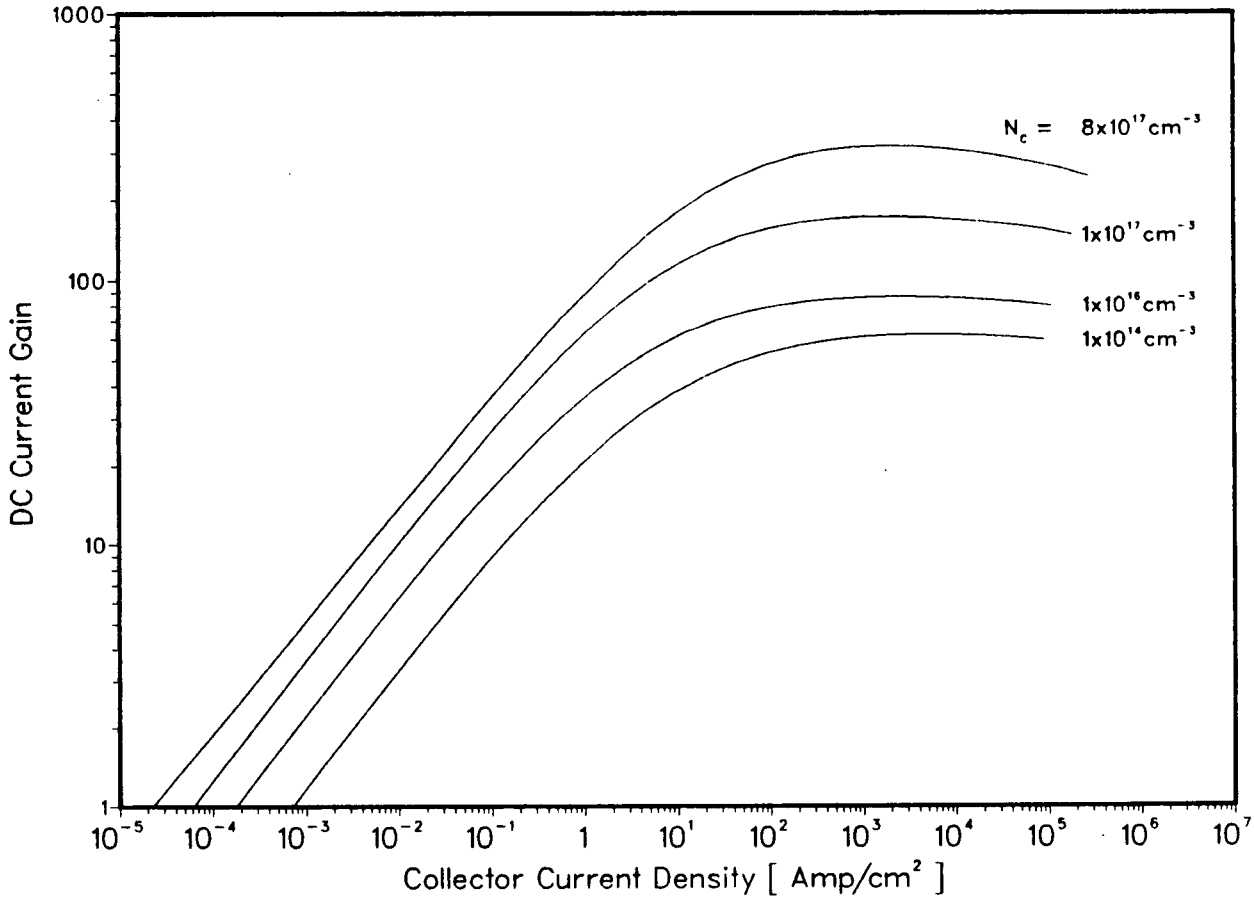

Fig. 2.16 The effect of collector doping on gain, as predicted by the analytical model using the parameters [other than N_C] listed in Table 2.3.

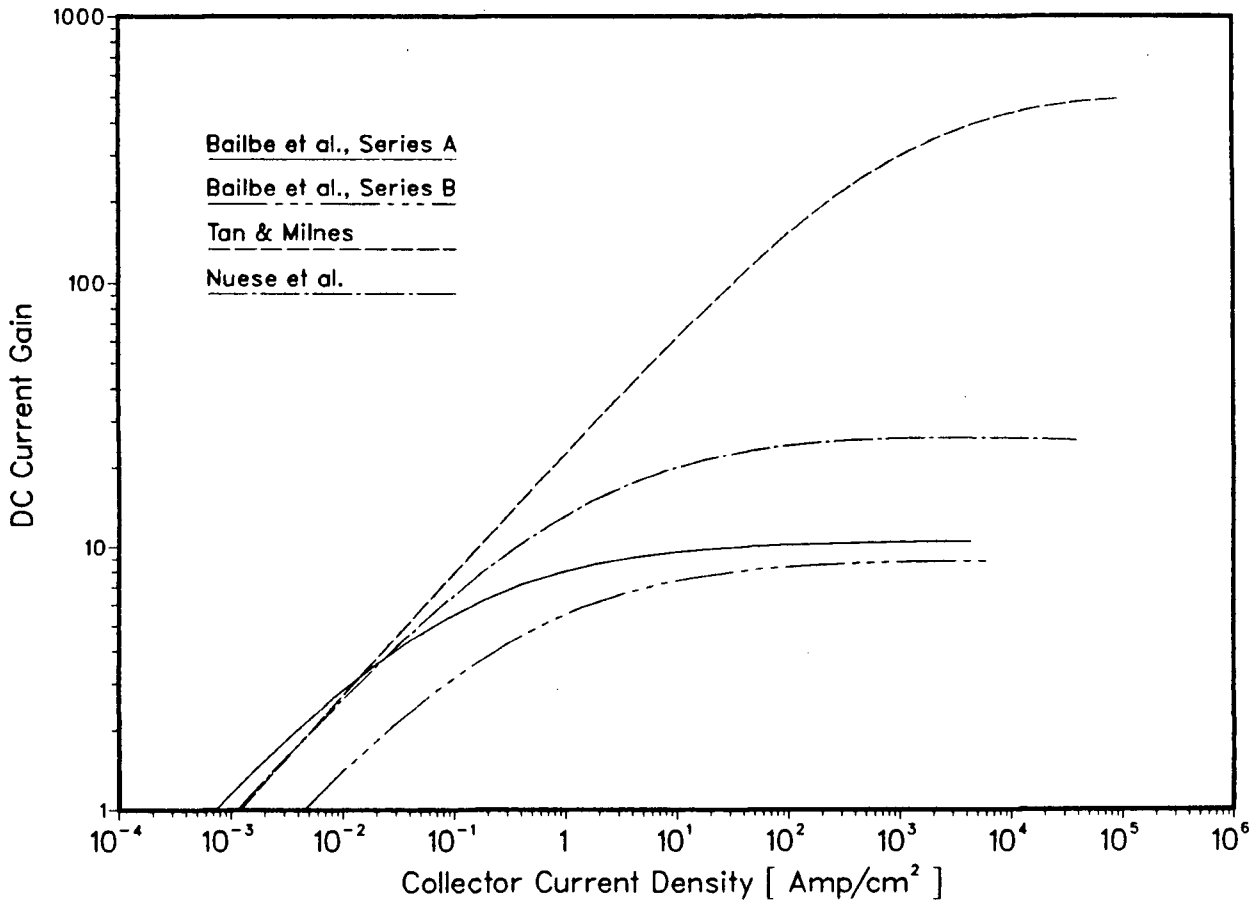

Fig. 2.17 The gain predicted by the analytical model using data for devices given by Bailbe et al. [35], Tan and Milnes [5] and Nuese et al. [12].

[35], prepared using LPE, and of Nuese et al. [12], prepared using VPE, are also shown in Figure 2.17. These devices also should possess uniformly doped semiconductor regions. The model predicts a gain of 25 for Nuese's devices, which is in accordance with their measured values of 30-90. In the case of Bailbe's devices, the measured gains are in the range of 12-25, which is somewhat higher than the values of 7-10 predicted by the model in Figure 2.17.

3. THE NUMERICAL MODEL

3.1 INTRODUCTION

The transistor model used in the analytical analysis in Chapter 2 assumes uniformly-doped emitter, base and collector regions. This model can only be applied to devices built by epitaxial processes. Most of the potentially practical GaAs homojunction bipolar transistors have been made so far by solid state diffusion or ion-implantation techniques, which lead to non-uniform spatial doping densities. Therefore the analytical approach will only provide an approximate prediction of the DC characteristics of these devices. In addition, the boundary conditions at both the base ends, the so-called junction law in the regional analysis [22], are known to become inaccurate under medium or high injection conditions. For a transistor with a high resistivity collector, the base boundary can be pushed beyond the metallurgical base-collector junction point into the collector region under high injection, resulting in a drastic decrease of cutoff frequency with increasing collector DC current (the Kirk Effect). Although only bipolars operating under low injection are considered in this work, the limitations imposed by the analytical approach point to the desirability of using numerical methods for a more accurate simulation of device behaviour.

The full numerical modeling of a semiconductor device, based on the five basic partial differential equations, the

continuity equations, the current transport equations and Poisson's equation was first suggested by Gummel [61] in 1964 for calculating the DC characteristics of a one-dimensional bipolar transistor. His approach was further developed and applied to a pn junction under both DC and transient conditions by De Mari [62] [63], and to IMPATT diodes by Schafetter and Gummel [64]. A two dimensional analysis of a bipolar transistor was presented by Slotboom in 1969 [65] by solving Poisson's equation and the continuity equations. At about the same time, two-dimensional solutions of Poisson's equation for a MOS structure were calculated by Loeb et al. [66] and Schroeder and Muller [67]. Since then, two dimensional steady state and transient modeling has been widely applied to various semiconductor devices such as JFET's, MOSFET's, MESFET's and thyristors. Recently, three dimensional static modeling has also been attempted on silicon MOSFET's [68-69].

In this analysis, the numerical model used is the one-dimensional model SEDAN (Semiconductor Device Analysis, Stanford University, January 1980 Version) [21]. SEDAN was primarily written for application to silicon devices. In this work, the model is applied to GaAs by making the appropriate changes to the model parameters such as the doping dependence of mobility, lifetimes and energy bandgap shrinkage pertinent to GaAs. The simulations focus on factors which are relevant to the recently published results for ion-implanted GaAs homojunction bipolar transistors

[14,15,17].

In using ion-implantation for device fabrication, there are some uncertainties concerning the actual distributions of the carriers in the device. The electrical activation of the implanted species varies with the dopant, the substrate material, the implant dose and energy, the encapsulant used to protect the GaAs surface during thermal annealing and the implant temperature. The indiffusion of impurities during high temperature annealing and the thickness of the masking layer also affect the final carrier profile. Therefore, as in the case of the analytical approach, some reasonable assumptions pertaining to these process-dependent parameters have to be made. Although it is difficult to perform a sensitivity analysis on the influence of each physical parameter on the device behaviour in SEDAN, a study of the DC transistor gain with different degrees of dopant activation, the influence of thermal dopant diffusion and bandgap narrowing is performed to establish the importance of these parameters on device performance. The simulation results of the ion-implanted transistors [14,15,17] are also compared to the measured values to show the accuracy of this model in predicting transistor static characteristics.

The succeeding sections of this chapter describe the numerical model and its related parameters needed in the computations performed with SEDAN, and also present the results and discussion of these simulations.

3.2 MODEL DESCRIPTION

3.2.1 BASIC EQUATIONS AND BOUNDARY CONDITIONS

SEDAN is based on the algorithm developed by Schafetter and Gummel [64] to solve self-consistently the five fundamental semiconductor differential equations: Poisson's equation, the continuity and current equations for electrons and holes, for the simultaneous solution of the electrostatic potential and the carrier concentrations. Under normal operating conditions, the DC characteristics of a bipolar transistor can be determined by knowing the electrostatic potential and the carrier concentration distribution. These basic equations in their one-dimensional, steady state form are as follows:

Poisson's Equation:

$$\frac{dE}{dx} = \frac{q}{\epsilon} (p - n + N_A - N_D) \tag{3.1}$$

Continuity Equations:

$$0 = U_p - \frac{1}{q} \frac{dJ_p}{dx} \tag{3.2}$$

$$0 = U_n + \frac{1}{q} \frac{dJ_n}{dx} \tag{3.3}$$

And the current equations:

$$J_p = q\mu_p pE - kT\mu_p \frac{dp}{dx} \tag{3.4}$$

$$J_n = q\mu_n nE + kT\mu_n \frac{dn}{dx} \tag{3.5}$$

where n and p are the electron and hole concentrations, N_D, N_A the donor and acceptor concentrations, ϵ the permittivity for GaAs, q the electronic charge and E the electric field intensity. J_n and J_p, U_n and U_p, and μ_n and μ_p are the electron and hole current density, generation-recombination rate, and mobility respectively. k is the well-known Boltzmann's constant.

It is assumed in SEDAN that both the emitter and collector contacts are ohmic and perfectly conducting, so there is no voltage drop at these boundaries. The electrostatic potential can then be given as the sum of the applied bias and the built-in voltage at these points, where the potential reference is taken at the emitter end. Thus,

$$\psi(0) = \frac{k.T}{q} \ln\left[\frac{n(0)}{n_i} \right] \tag{3.6}$$

$$\psi(R) = V_{CE} + \frac{k.T}{q} \ln\left[\frac{n(R)}{n_i} \right] \tag{3.7}$$

$\psi(0)$, $\psi(R)$ and n(0), n(R) are the electrostatic potential and electron concentration at the emitter and collector ends, respectively, n_i is the intrinsic carrier

concentration of GaAs and is assigned a value of 2×10^6 cm^{-3}. To determine the boundary conditions for the carrier concentrations, thermal equilibrium and zero space charge are assumed to exist at the contact ends, therefore:

$$n(0)p(0) = n_i^2 \tag{3.8a}$$

$$n(R)p(R) = n_i^2 \tag{3.8b}$$

$$p(0) - n(0) + C(0) = 0 \tag{3.8c}$$

$$p(R) - n(R) + C(R) = 0 \tag{3.8d}$$

where

$$C(x) = N_D(x) - N_A(x) \tag{3.8e}$$

Equations (3.8a)-(3.8d) can be rearranged into Dirichlet boundary conditions for electrons and holes:

$$n(0) = \frac{\sqrt{\{ C(0)^2 + 4n_i^2 \}} + C(0)}{2} \tag{3.9a}$$

$$p(0) = \frac{\sqrt{\{ C(0)^2 + 4n_i^2 \}} - C(0)}{2} \tag{3.9b}$$

$$n(R) = \frac{\sqrt{\{ C(R)^2 + 4n_i^2 \}} + C(R)}{2} \tag{3.9c}$$

$$p(R) = \frac{\sqrt{\{ C(R)^2 + 4n_i^2 \}} - C(R)}{2} \qquad (3.9d)$$

where p(0) and p(R) are the equilibrium hole concentrations at the emitter and collector contacts respectively.

The recombination-generation process is assumed to be dominated by the Shockley-Read-Hall type of mechanism for single energy level recombination-generation centers, so U_n and U_p are expressed as:

$$U_n = U_p = \frac{pn - n_i^2}{\tau_{no}(n+n_1) + \tau_{po}(p+p_1)} \qquad (3.10)$$

where p_1, n_1 are the hole and electron concentrations in the conduction band when the Fermi level coincides with the energy level of the recombination-generation center, and τ_{no}, τ_{po} are the hole and electron lifetimes in n-type, p-type material respectively.

3.2.2 THE PHYSICAL PARAMETERS

The physical parameters are formulated following a similar approach to that used in the analytical model. The doping dependence of the minority carrier lifetimes τ_{po} and τ_{no} is described by equation (2.51), with the appropriate polynomial coefficients and dependent variables given in Table 2.2. The field-dependent mobility is expressed by the empirical relation [70]:

$$\mu = \frac{\mu^*}{1 + \frac{\mu^*}{v_s} E} \qquad (3.11)$$

Where μ^* is the low field mobility, and its doping dependence is derived in equations (2.47-2.48) for electrons and (2.47-2.50) for holes, with the polynomial coefficients given in Table 2.1. E is the electric field and the saturation velocity v_s is taken as 1.0×10^7 cm/sec for both electrons and holes [71].

The effect of heavy doping on the energy bandgap narrowing is related to the effective intrinsic carrier concentration n_{ie}, which is described in equations (2.38-2.41). The activation energy of the impurity dopants is assumed to be zero to be consistent with the setup of SEDAN as used in silicon device modeling.

3.2.3 ION IMPLANTATION PARAMETERS

Ion implantation is a doping technique which is widely used in integrated circuit device fabrication. It offers a precise control over the impurity density and depth profile. As such, narrow basewidths in bipolar transistors can be achieved with this method. By implanting a dopant into GaAs, the lattice damage produced by the high energy ions results in a degradation of the minority carrier lifetime, due to excess recombination in the material. It has been shown that by utilising a suitable annealing scheme, these lattice

disorders can be removed [72], hence recovering the lifetime of the implanted layer. As discussed in the analytical model in Chapter 2, narrow basewidths and long base lifetimes are the parameters required to achieve superior DC performance in GaAs bipolars. Therefore, ion-implantation should be a very helpful technique in the realisation of high gain devices.

The doping profile due to ion-implantation is approximated by a one-dimensional symmetric Gaussian distribution function according to the theory of Lindhard, Scharff, and Schiøtt (LSS) [73]:

$$N(x) = \frac{Q_0}{\sqrt{(2\pi).\Delta R_P}} \exp\left[- \frac{(x-R_P)^2}{2.\Delta R_P^2} \right] - N_A \qquad (3.12)$$

where Q_0 is the implant dose, N_A the background impurity concentration, R_P the mean value or projected range and ΔR_P the standard deviation or straggle of the normal distribution. The LSS theory is a first order approximation to the actual doping profile, but is considered adequate in our application. Higher order effects such as the exponential decaying tails observed in some actual implant profiles do not affect the overall distribution, and hence the device performance.

To calculate the doping profile using equation (3.12), it is necessary to have knowledge of R_P and ΔR_P under given implant conditions. Tables of projected range and standard deviations computed by Gibbons et al. [74] and Ryssel and

Ruge [75] were used for silicon, selenium, and beryllium implants into GaAs. As the tables are inconvenient to use and do not provide all the required R_p's and ΔR_p's under the implantation scheme outlined in Table 3.1, a functional fit to the tabulated data has been performed. The fitted curves are low order, simple least square polynomials, as suggested by Selberherr et al. [76], and have the forms:

$$R_p = \sum_{i=0}^{n} a_i . E^i \qquad (3.13)$$

$$\Delta R_p = \sum_{i=0}^{n} b_i . E_i \qquad (3.14)$$

where a_i, b_i are the coefficients of the fitted curves in micrometers and E is the implant energy in keV. These coefficients are listed in Table 3.2 and Table 3.3 for the various elements. The non-vanishing a_0 and b_0 are necessary in the construction of the polynomial functions to minimize the root-mean square errors. The maximum error approximated by equations (3.13) and (3.14) is less than 2% when compared to the tabulated values in [74], [75] for an implant energy range of 20 - 500 keV. The fitted curves of R_p, ΔR_p versus implant energy are shown in Figure 3.1 and Figure 3.2.

The high temperature annealing steps following implantation result in diffusion of dopants into the substrate. It has been shown that for low-dose Be, Si and Se implants ($\leq 1 \times 10^{14}$ cm^{-2}) there is very limited diffusion and the carrier profile agrees with the Gaussian

Ref	Ion	Capping (depth)	Subst. temp(°C)	Energy (keV)	Dose (cm^{-2})	Anneal temp, time(°C,min)
[14]	Be	Si_3N_4 (400Å)	RT	250	$3x10^{12}$	850,30
		Si_3N_4 (400Å)	RT	130	$2x10^{12}$	850,30
		Si_3N_4 (400Å)	RT	90	$9x10^{11}$	850,30
	Si	Si_3N_4 (400Å)	RT	150	$2x10^{14}$	850,30
[15]	Se	none	350	360	$5x10^{13}$	850,30
	Be	none	RT	125	$6x10^{12}$	700,30
[17]	Se	Si_3N_4	350	150	$1x10^{13}$	850,30
		Si_3N_4	350	360	$2x10^{13}$	850,30
	Be	Si_3N_4	RT	180	$6x10^{12}$	800,30

Table 3.1 Implantation schedule used in Refs. [14,15,17] for fabricating GaAs n-p-n bipolar transistors.

Dopant	Silicon	Selenium	Beryllium
a_0	2.76×10^{-3}	3.00×10^{-3}	-7.44×10^{-3}
a_1	7.55×10^{-4}	3.80×10^{-4}	3.31×10^{-4}
a_2	8.991×10^{-7}	-5.974×10^{-7}	1.782×10^{-7}
a_3	-2.56×10^{-9}	2.60×10^{-9}	-1.14×10^{-8}
a_4	3.24×10^{-12}	-4.78×10^{-12}	2.56×10^{-11}
a_5	-1.66×10^{-15}	3.26×10^{-15}	-1.91×10^{-14}

Table 3.2 Coefficients for R_p in equation (3.13).

Dopant	Silicon	Selenium	Beryllium
b_0	2.84×10^{-3}	1.59×10^{-3}	1.00×10^{-2}
b_1	4.95×10^{-4}	1.96×10^{-4}	2.08×10^{-3}
b_2	-1.005×10^{-6}	-4.623×10^{-7}	-1.04×10^{-5}
b_3	2.32×10^{-9}	1.60×10^{-9}	3.25×10^{-8}
b_4	-3.54×10^{-12}	-2.82×10^{-12}	-5.28×10^{-11}
b_5	2.27×10^{-15}	1.90×10^{-15}	3.39×10^{-14}

Table 3.3 Coefficients for ΔR_p in equation (3.14).

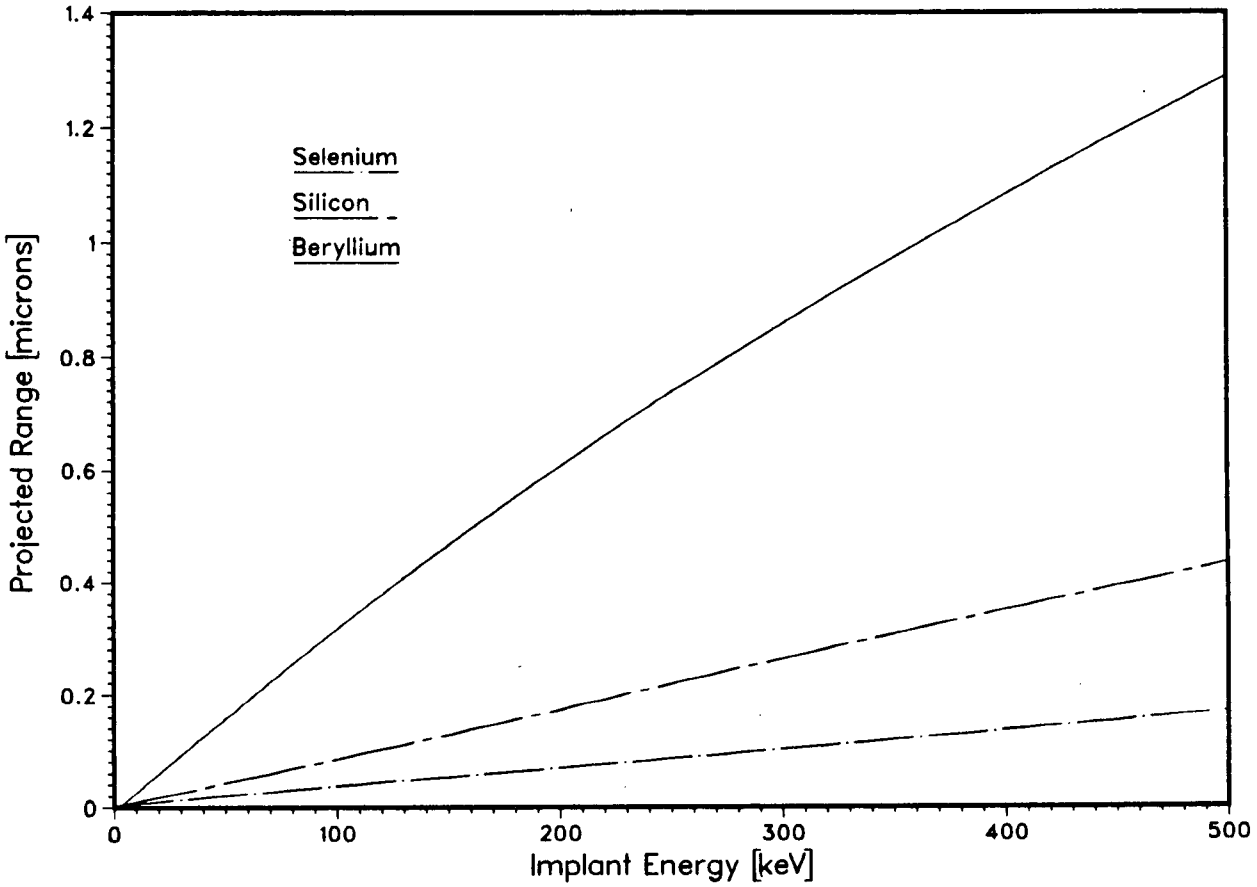

Fig. 3.1 Projected range versus implant energy for selenium, silicon and beryllium in GaAs.

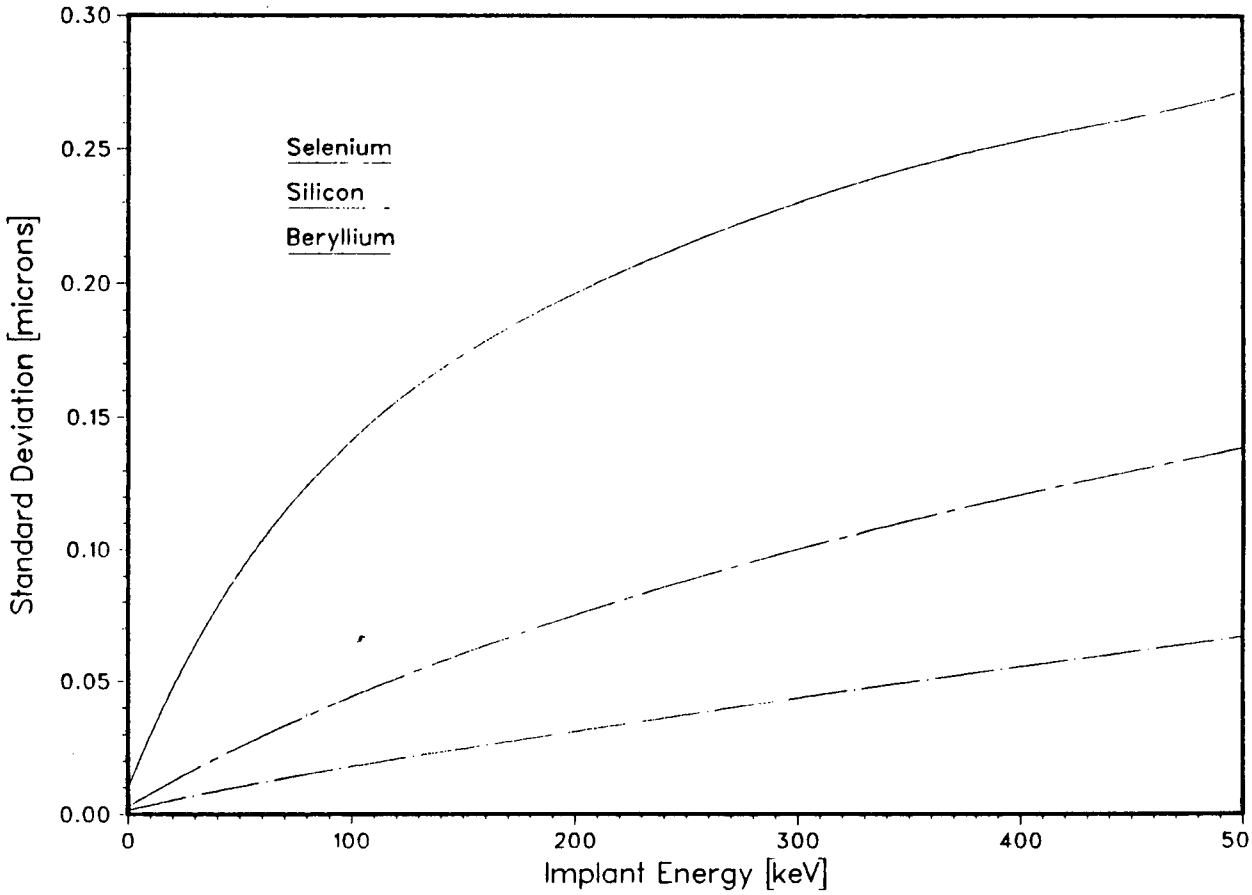

Fig. 3.2 Standard deviation versus implant energy for selenium, silicon and beryllium in GaAs.

distribution when adjusted with an appropriate activation efficiency [77]. For high-dose implants and annealing temperatures greater than 800°C, considerable diffusion takes place, and a broader normal distribution is obtained [77]. To account for the diffusion effects, the standard deviation in equation (3.12) is modified to an effective form [78]:

$$\Delta R_{Peff} = \sqrt{\{ 2.\sum_{i=0}^{n} D_i.t_i + \Delta R_P^2 \}} \qquad (3.15)$$

where D_i and t_i are, respectively, the appropriate diffusion constant and anneal time for the ith anneal step. From Table 3.1, only the devices from Hughes [14] employ high-dose silicon implants for the n^+ emitter, therefore equation (3.15) is needed to calculate the doping profile of these devices. The diffusion constant of silicon at 850°C is taken as 3.3×10^{14} cm^2 sec^{-1} as determined from the analysis of the carrier concentration profile for a Si-implanted LPE buffer substrate [79].

The capping material used during implantation for the protection of the GaAs surface, such as the Si_3N_4 layer used in [14], can affect the profile as well. This effect can be included by introducing a truncated Gaussian distribution, in which R_P is changed to [80]:

$$R_{Peff} = R_P - t_{cap} \qquad (3.16)$$

where t_{cap} is the thickness of the capping layer.

For ion-implanted material, the actual amount of dopant that goes into substitutional sites to become electrically active during annealing depends on a number of factors such as the anneal temperature and dose used. The ratio of sheet carrier concentration of an annealed sample and the implant fluence used is the activation efficiency and is given as [81]:

$$\eta = \frac{N_s}{Q_o} \tag{3.17}$$

where N_s is the sheet carrier concentration of the sample.

The doping function using LSS theory, taking into consideration the effects of dopant diffusion, capping and carrier activation is given, following equation (3.12), as:

$$N(x) = \eta \cdot \frac{Q_o}{\sqrt{(2\pi)}.\Delta R_{Peff}} \exp\left[\frac{(x-R_{Peff})^2}{2\Delta R_{Peff}^2} \right] - N_A \tag{3.18}$$

Assuming zero activation energy for the implanted dopants, the carrier profile is then described by equation (3.18).

3.3 SOLUTION PROCEDURE USING SEDAN

To perform a bipolar transistor simulation using SEDAN, a data file containing the necessary input information has to be provided. These input specifications include:

(1) The dividing of the one-dimensional transistor structure into various regions, where each region is assigned a unique grid spacing. In this case, the regions are the neutral widths of the emitter, base, collector and the two junction depletion layers. To select the grid points for each region, a trial and error method is employed until a convergence of the solution is obtained. In general, fine grid spacings of about 0.01 μm to 0.005 μm are needed for very steep profiles, and grid spacings of 0.1 μm are sufficient for constant or slowly varying profiles. For devices with very narrow bases, there must be enough grid points in the base to ensure the convergence and accuracy of the solution.

(2) The selection of a reference point for the base contact. The mid-point of the metallurgical base is normally used. However, in choosing the base contact point, care must be taken to ensure that this location does not extend into the base-emitter or base-collector depletion regions for a given bias, or the solution will fail to converge.

(3) The range, straggle and peak value for the Gaussian profile for each implanted dopant. The range and straggle data are computed using equations (3.13)-(3.14) with the appropriate polynomial coefficients from Tables 3.1 and 3.2. The peak carrier concentration value is obtained from equation (3.18) by setting $x = R_{Peff}$.

(4) The bias voltage V_{BE}, and its incremental value for a

fixed emitter-collector voltage, V_{CE}. The initial and final values of V_{BE} are taken to be 0.6 V and 1.30 V, respectively, and V_{CE} is set equal to 4.0 V.

(5) The desired outputs, such as plots of β versus J_C.

On providing the necessary information, SEDAN will then generate the required outputs.

3.4 RESULTS AND DISCUSSION

In this numerical analysis, the simulation of the performance of two device structures built by different fabrication procedures is investigated. In the Hughes process [14], evaporated, heavy metal masks were used to enable selective implants into an n-type GaAs epitaxial layer grown on an n^+ substrate. A multiple Be implant was used for the base formation and a high dose silicon implant for the emitter. The annealing for both implanted species was carried out simultaneously at 850°C for 30 minutes. The implantation parameters and conditions are given in Table 3.1. For GaAs implanted with beryllium, full electrical activation of the dopant has been obtained at an annealing temperature as low as 600°C [82]. Therefore the activation of the beryllium is taken to be 100%. For the silicon implant dose of 2×10^{14} cm^{-2}, the value of its activation efficiency has been determined to vary from 3.2% to 30% [79], and considerable diffusion of carriers occurs at the annealing temperature of 850°C [77]. The effect of the silicon activation and indiffusion, using a diffusion

constant of 3.3×10^{14} cm^2 sec^{-1} [79], on the doping profile for the Hughes fabrication routine is shown in Figure 3.3. The variations in activation efficiency and diffusion cause a change in the effective widths of the base and emitter regions. From Figure 3.3, it can be seen that for a silicon activation efficiency of 15%, the carrier indiffusion results in a considerable narrowing of the basewidth of the device. Therefore, a device that has a carrier profile modified by the diffusion effect would be expected to exhibit higher current gain. The results predicted by SEDAN for the Hughes device structure are shown in Figure 3.4. From the figure, the maximum gain obtained varied over the range of 8-30, depending on the value of the activation efficiency and whether or not the indiffusion effect was included. This is in good agreement with the measured values of 7-25 for the Hughes experimental devices [14]. The effect of bandgap narrowing on the device performance is also shown in Figure 3.4. The effect is substantial and, for the example shown of a silicon activation of 15%, bandgap narrowing serves to reduce the predicted β_{max} value from 80 to 14. It is speculated in [14] that the low measured values of current gain for these experimental devices are due to the effect of "surface leakage". However, the close agreement between the model results presented here and the measured data suggest that the low gains attained are, in fact, due to intrinsic phenomena, such as device geometry, doping densities and material properties, with bandgap

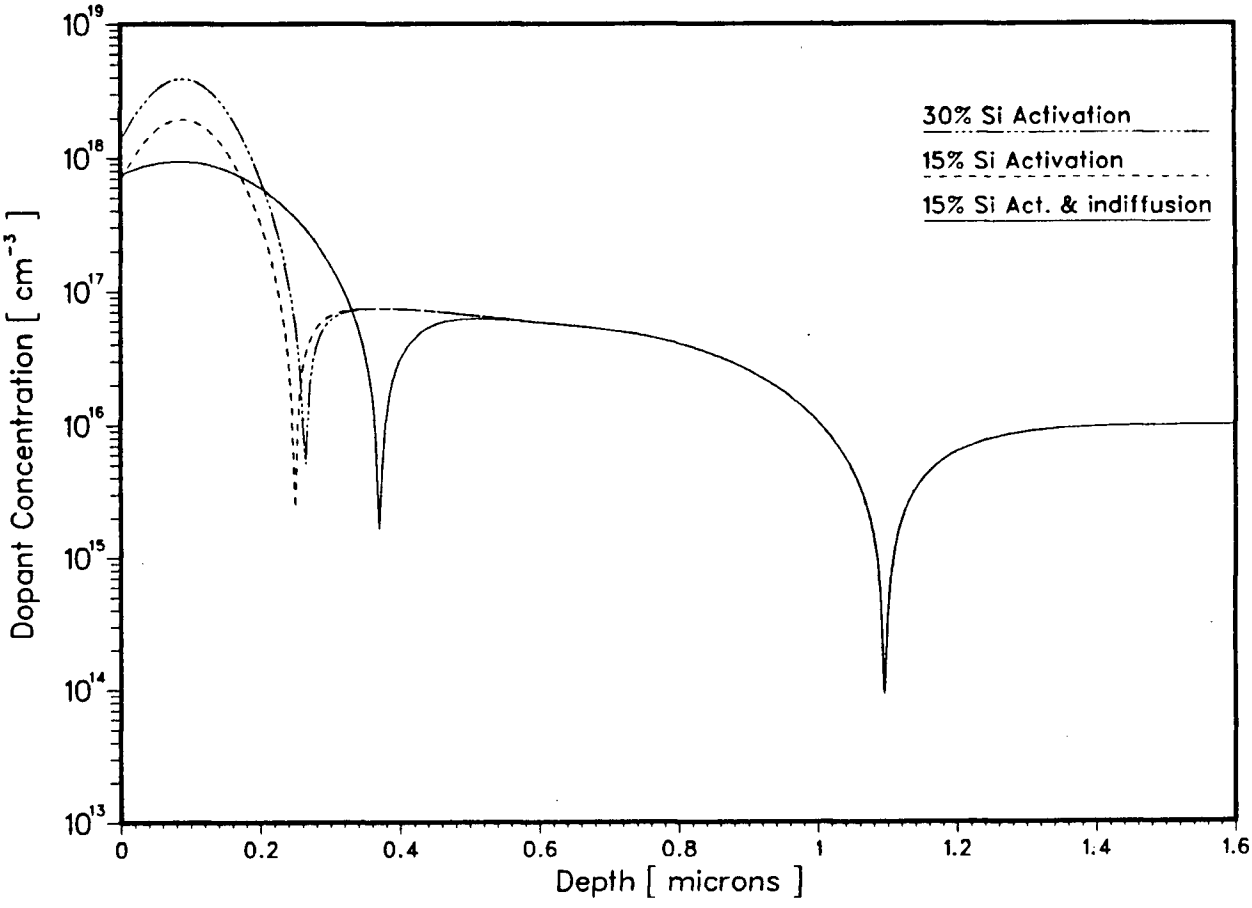

Fig. 3.3 The computed doping profile for the Hughes device structure [14], showing the effect of activation efficiency and in-diffusion for the implanted Si species.

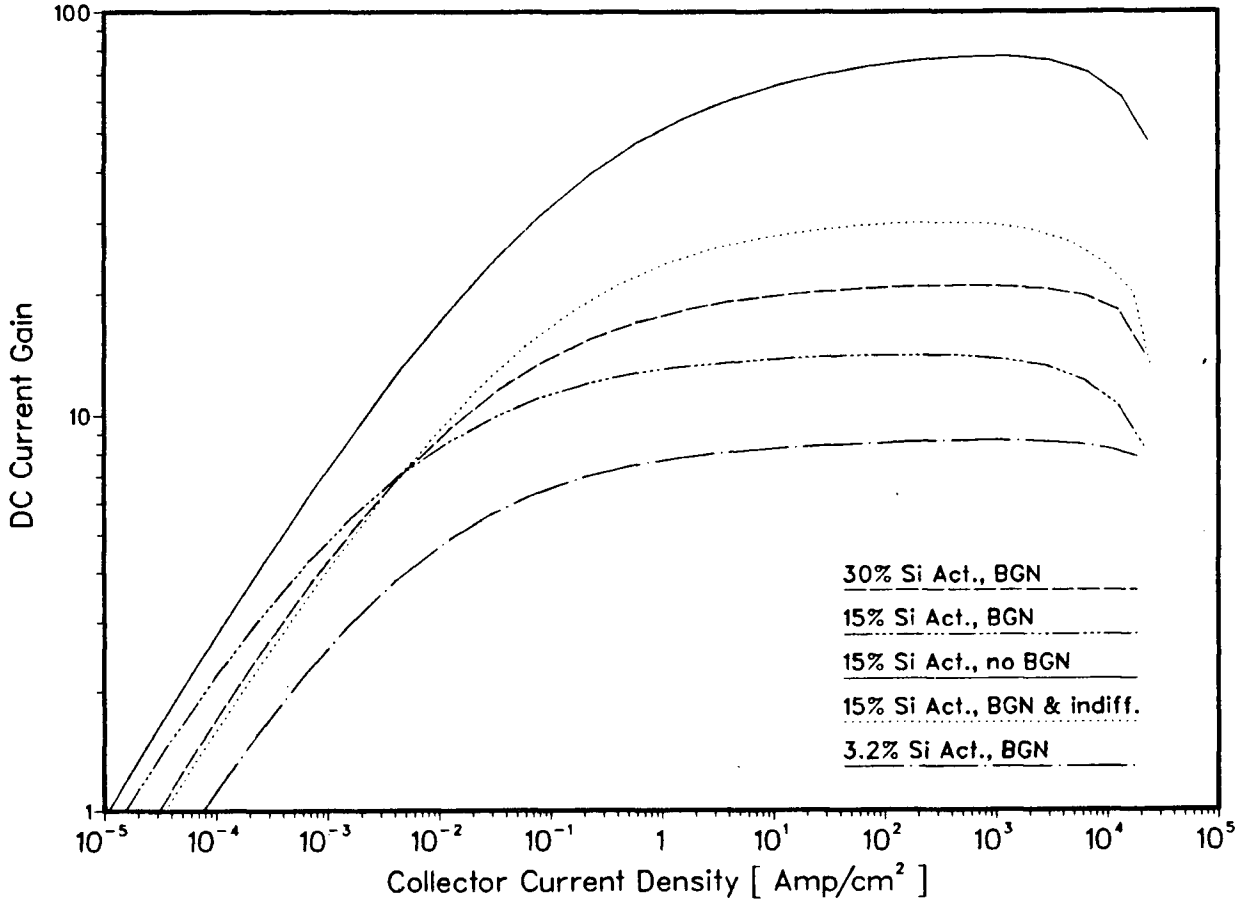

Fig. 3.4 The effect of silicon activation efficiency, silicon in-diffusion and bandgap narrowing (BGN) on gain for the Hughes device structure [14], as predicted by the numerical model.

narrowing being particularly important.

In the Texas Instrument fabrication sequence, unmasked implantations are used for the base and emitter regions, and boron implantation is used to achieve device isolation. A single Se implant was used for the emitter formation in the device described in [15], while a double Se implant was employed in the devices considered in [17]. For both transistors, a single Be implant was used for the base region. Separate base and emitter annealing was performed and the implantation parameters are given in Table 3.1. The calculated doping profiles for both device structures are shown in Figure 3.5. The doping profile for the double Se implant device [17] has been computed by assuming a 70% activation of the implanted selenium and 100% activation of the implanted beryllium. This provides good agreement with the peak carrier doping concentration, and the emitter and basewidths resulting from the profile calculated by Doerbeck et al. [17], who used the LSS Gaussian distribution, suitably modified by experimentally observed, but unspecified, activation efficiencies. An attempt was made to model the redistribution of the impurities from the n^+ substrate due to out-diffusion into the undoped epitaxial layer of the device in [17]. The measured profile after re-distribution was deduced from C-V measurements [17]. An error function profile, as used elsewhere for the impurity redistribution from a buried layer [83], was employed, namely:

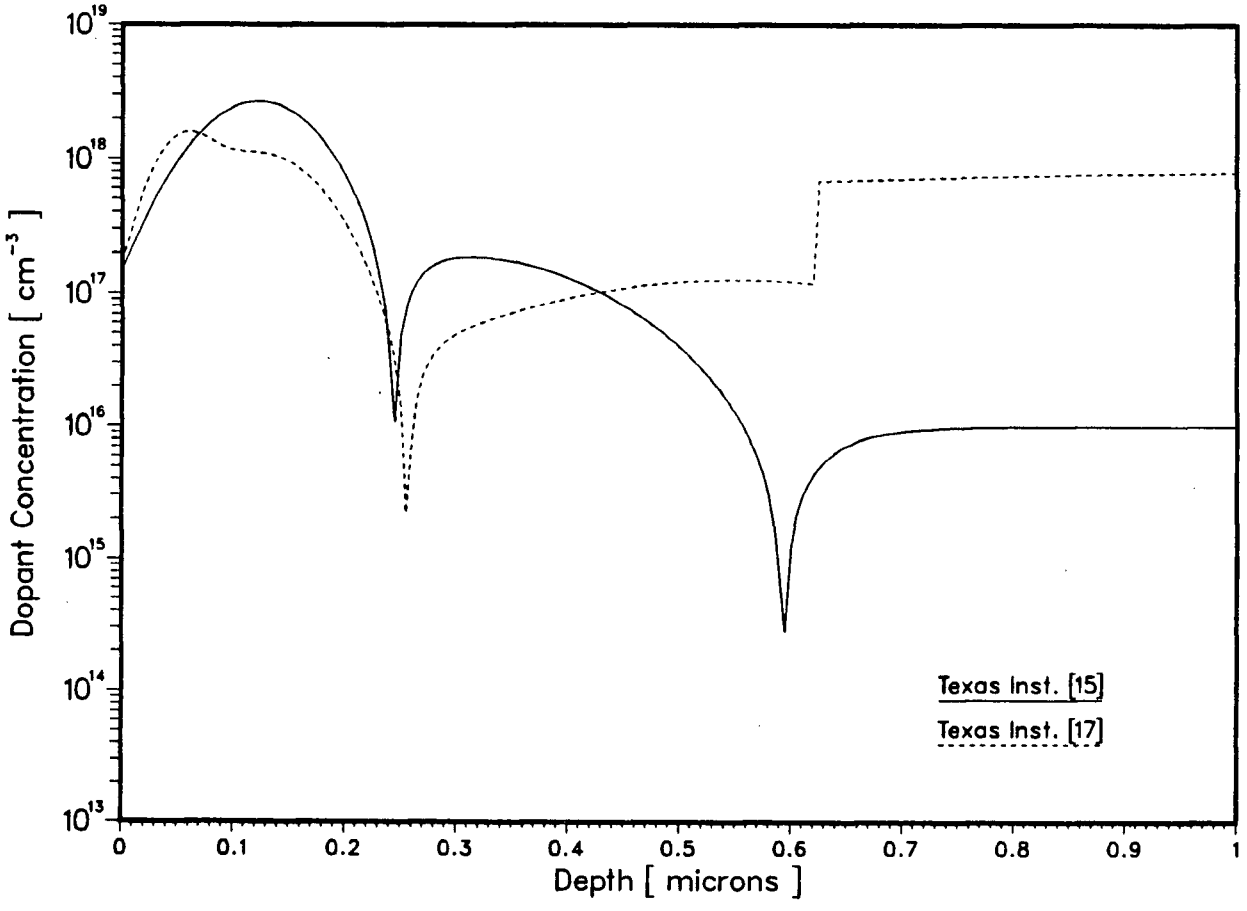

Fig. 3.5 The computed doping profile for the Texas Instrument device structures of Refs. [15,17], assuming 70% activation of the implanted selenium and 100% activation of the implanted beryllium. The redistribution of impurities in the epitaxial collector of the device [17] is represented by an abrupt profile.

$$N(x,t) = \frac{N^+}{2} \{ \mathrm{erfc}[\frac{-x}{2\sqrt{(Dt)}}] - \mathrm{erfc}[\frac{x^+ - x}{2\sqrt{(Dt)}}] - \mathrm{erfc}[\frac{2.x_{epi} - x^+ + x}{2\sqrt{(Dt)}}] + \mathrm{erfc}[\frac{2.x_{epi} + x}{2\sqrt{(Dt)}}] \} \quad (3.19) .$$

where N^+ is the doping concentration of the buried substrate, x^+ is the thickness of the buried layer, x_{epi} is thickness of the epitaxial layer, and D and t are the diffusion constant and diffusion time, respectively. However, the profile generated from equation (3.19) bore little resemblance to the measured distribution. Thus, in the results that follow, an abrupt profile with a doping density of $8x10^{17}$ cm^{-3} in the collector is assumed, as shown in Figure 3.5.

The doping profile for the device in Reference [15] with the single Se implant was also computed by assuming 70% Se implant activation and 100% beryllium implant activation. This is justifiable as the implant conditions are basically similar for both device structures [15], [17], as can be seen from Table 3.1. The epitaxial layer for the single implant device had a doping density of $1x\ 10^{16}$ cm^{-3}, which is assumed to be constant in the profile calculation, as indicated in Figure 3.5.

The computed results for both device structures based on the carrier profiles in Figure 3.5 are shown in

Figure 3.6. The computed β_{max} of the device in [15] is 18, which is somewhat higher than the measured value of 8, while the predicted β_{max} for the device with the two Se implants [17] is 35, which is in good agreement with the measured values of 20-30.

The Texas Instrument devices [15,17] exhibit higher emitter peak doping densities and narrower basewidths than the Hughes devices [14]. However, the DC performances are not very different. This suggests that the emitter is playing an important role in determining the gain of TI's devices. From a comparison of Figures 3.3. and 3.5, it can be appreciated that the TI process leads to a narrower emitter than that exhibited by the Hughes devices for which Si indiffusion is significant. The two values of W_E are approximately 0.4 μm and 0.25 μm respectively. Figure 2.13 indicates that such a difference in the emitter width has a considerable effect on β_{max}. Comparison of the results from Figure 2.13 with those from the numerical model is appropriate in this case as the value of $s_F = 2x10^6$ cm/sec used in computing Figure 2.13 is sufficiently high to adequately represent the ohmic contact assumed in the numerical model. This suggests that a significant improvement in performance of the TI devices could be achieved by seeking a reduction in the effect of surface recombination at the emitter front.

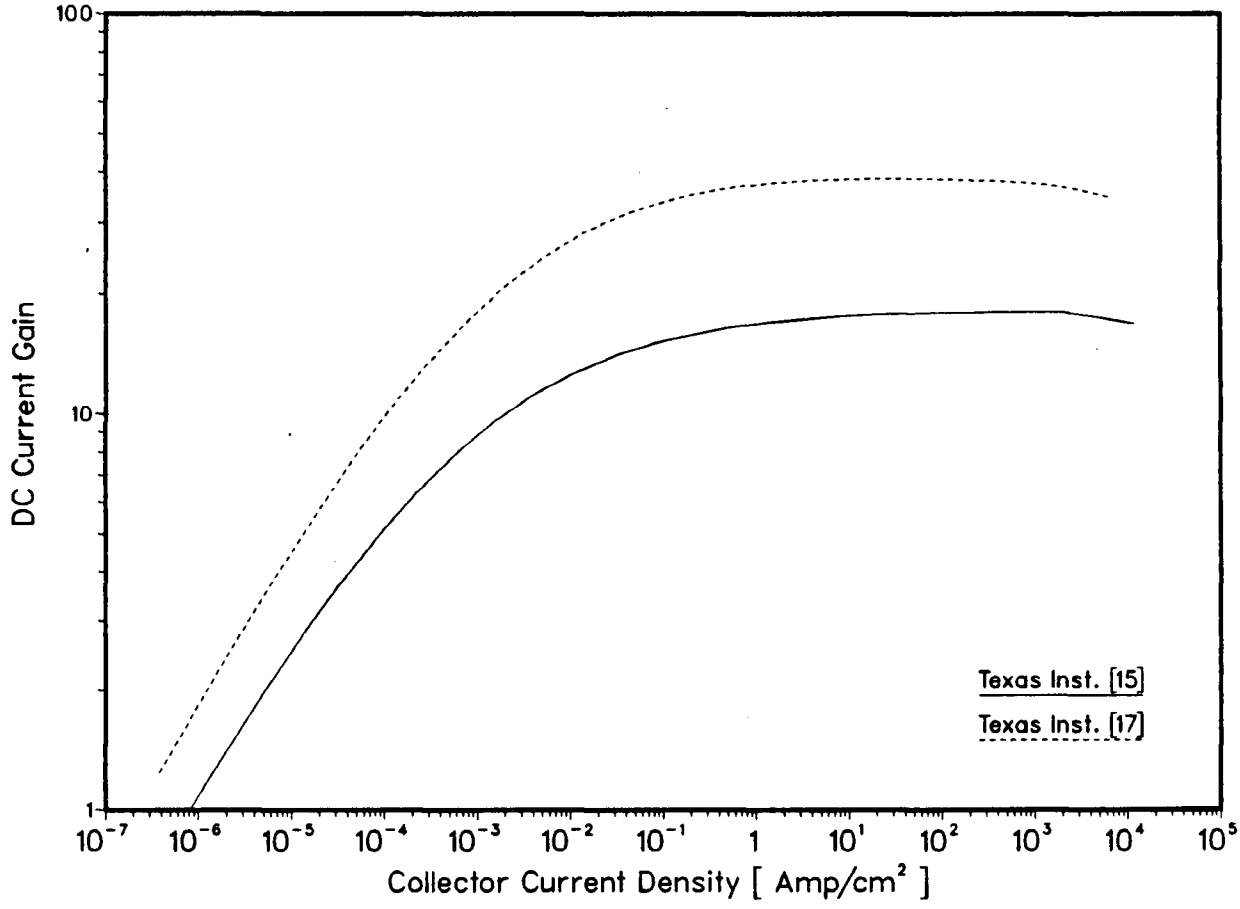

Fig. 3.6 The computed gain for the Texas Instrument device structures of Refs. [15,17], assuming 70% activation of the implanted selenium and 100% activation of the implanted beryllium.

4. CONCLUSIONS

The analytical model developed for the npn GaAs homojunction bipolar transistors has been shown to be useful in predicting gains for previously-reported devices fabricated by MBE, VPE and LPE techniques, which are considered to have uniformly-doped emitter, base and collector regions. It has also been shown that the measured gains of about 10-90 which have been reported for these devices are to be expected from the device geometries and doping densities employed.

The analytical model has also proved useful in examining the sensitivity of the gain to the variation of the device parameters. The conclusion that can be drawn from the analysis, is that a high gain transistor, with a β of the order of 1000, would require a narrow basewidth ($\leq 0.2\ \mu m$), lightly doped base ($\leq 10^{17}\ cm^{-3}$) as well as a narrow emitter width ($\leq 0.25\ \mu m$) and a surface recombination velocity of less than 10^4 cm/sec. The geometrical and doping features should be easily attainable in practice but the required low surface recombination velocity may be more difficult to achieve. The passivation of GaAs surfaces is a subject worthy of further study.

The numerical model developed here has been shown to be useful in predicting gains for ion-implanted GaAs transistors. The agreement with experimental data is good, provided that the bandgap narrowing effect is taken into consideration. This suggests that the DC performance of the

devices fabricated thus far is limited by intrinsic phenomena, and not by extraneous effects such as surface leakage which have been claimed in the literature. For devices with good base properties, emitter surface effects appear to limit the performance of the device. Further improvements in gain would appear to demand, as in the devices mentioned earlier which were fabricated by epitaxial techniques, a reduction of these effects, principally by enhancing passivation of the emitter surface.

REFERENCES

[1] R. C. Eden, B. M. Welch, R. Zucca, and S. I. Long, "The prospects for ultrahigh-speed VLSI GaAs digital logic," *IEEE Trans. Electron Devices*, vol. ED-26, no. 4, pp. 299-317, 1979.

[2] R. C. Eden and B. M. Welch, "Ultra high speed GaAs VLSI: Approaches, potential and progress," in *VLSI Electronics: Microstructure Science* (edited by N. Einspruch), pp. 109-162, vol. 3, Academic Press, New York, 1981.

[3] H. Kroemer, "Heterostructure bipolar transistors and integrated circuits," *Proc. IEEE*, vol. 70, no. 1, pp. 13-25, 1982.

[4] R. C. Eden, "Comparison of GaAs device approaches for ultrahigh-speed VLSI," *Proc. IEEE*, vol. 70, no. 1, pp. 5-12, 1982.

[5] S. S. Tan and A. G. Milnes, "Consideration of the frequency performance of GaAs homojunction and heterojunction n-p-n transistors," *IEEE Trans. Electron Devices*, vol. ED-30, no. 10, pp. 1289-1294, 1983.

[6] G. R. Antell, "Gallium Arsenide Transistors," in *Semiconductors and Semimetals* (edited by R. K. Willardson and A. C. Beer), vol. 7, part A, pp. 273-292, Academic Press, New York, 1971.

[7] H. Becke, H. Flatley, and D. Stolnitz, "Double diffused Gallium Arsenide transistors," *Solid-State Electron.*, vol. 8, pp. 255-265, 1965.

[8] W. Von Münch, H. Statz, and A. E. Blakeslee, "Isolated GaAs transistors on high-resistivity GaAs substrate," *Solid-State Electron.*, vol. 9, pp. 826-827, 1966.

[9] W. Von Müench and H. Statz, "Solid-to-solid diffusion in the Gallium Arsenide device technology," *Solid-State Electron.*, vol. 9, pp. 939-942, 1966.

[10] G. R. Antell and A. P. White, "Double diffused gallium arsenide transistor," *Int. Symp. Gallium Arsenide* [*Conf. Ser.-Inst. Phys.*], pp. 201-205, 1966.

[11] H. Strack, "Iron-doped gallium arsenide transistors," *Int. Symp. Gallium Arsenide* [*Conf. Ser.-Inst. Phys.*], pp. 206-212, 1966.

[12] C. J. Nuese, J. J. Gannon, R. H. Dean, H. F. Gossenberger, and R. E. Enstrom, "GaAs vapor-grown bipolar transistors," *Solid-State Electron.*, vol. 15, pp. 81-91, 1972.

[13] K. V. Vaidyanathan, R. A. Jullens, C. L. Anderson, and H. L. Dunlap, "Planar, ion-implanted GaAs bipolar transistors," *Tech. Dig. IEEE IEDM*, p. 826, 1980.

[14] -------, "Planar, ion-implanted bipolar devices in GaAs," *Solid-State Electron.*, vol. 26, no. 8, pp. 717-721, 1983.

[15] H. T. Yuan, F. H. Doerbeck, and W. V. Mclevige, "Ion implanted GaAs bipolar transistors," *Electron. Lett.*, vol. 16, no. 16, pp. 637-638, 1980.

[16] H. T. Yuan, W. V. Mclevige, F. H. Doerbeck, and E. G. Dierschke, "GaAs bipolar integrated circuit technology," *Tech. Dig. IEEE IEDM*, pp. 398-400, 1980.

[17] F. H. Doerbeck, W. M. Duncan, W. V. Mclevige, and H. T. Yuan, "Fabrication and high-temperature characteristics of ion-implanted GaAs bipolar transistors and ring oscillators," *IEEE Trans. Ind. Electron.*, vol. IE-29, no. 2, pp. 136-139, 1982.

[18] H. Krautle, P. Narozny, and H. Beneking, "Lateral pnp GaAs bipolar transistor prepared by ion implantation," *Electron. Lett.*, vol. 18, pp. 259-260, 1982.

[19] -------, "Lateral PNP GaAs bipolar transistor with minimized substrate current," *IEEE Electron Devices Lett.*, vol. EDL-3, no. 10, pp. 315-317, 1982.

[20] K. V. Vaidyanathan, C. L. Anderson, H. L. Dunlap, and R. A. Jullens, "Ion implantation of wide bandgap semiconductors," Final Report, Contract No. N001-73-79-C-0028, Naval Electronics Systems Command, Washington, D.C. 20375.

[21] Massimo Vanzi, *Semiconductor Device Analysis* Program, Integrated Circuits Laboratory, Stanford University, January 1980 Version.

[22] M. Kurata, *Numerical Analysis for Semiconductor Devices*, p. 3, D. C. Heath and Company, Lexington, Massachusetts, 1982.

[23] S. C. Choo, "Carrier generation-recombination in the space-charge region of an asymmetrical p-n junction," *Solid-State Electron.*, vol. 11, pp. 1069-1077, 1968.

[24] C. T. Sah, R. N. Noyce, and W. Shockley, "Carrier generation and recombination in P-N junctions and P-N junction characteristics," *Proc. IRE*, vol. 45, pp. 1228-1243, 1957.

[25] A. M. Sekela, D. L. Feucht, and A. G. Milnes, "Diffusion length studies in n gallium arsenide," *Gallium Arsenide and Related Compounds* [*Conf. Ser.-Inst. Phys.*], no. 24, pp. 245-253, 1975.

[26] R. D. Ryan and J. E. Eberhardt, "Hole diffusion length in high purity n-GaAs," *Solid-State Electron.*, vol. 15, pp. 865-868, 1972.

[27] H. C. Casey, Jr., B. I. Miller, and E. Pinkas, "Variation of minority-carrier length with carrier concentration in GaAs liquid-phase epitaxial layers," *J. Appl. Phys.*, vol. 44, no. 3, pp. 1281-1286, 1973.

[28] H. C. Casey, Jr. and F. Stern, "Concentration-dependent absorption and spontaneous emission of heavily doped GaAs," *J. Appl. Phys.*, vol. 47, no. 2, pp. 631-643, 1976.

[29] A. G. Milnes, "Impurity levels in gallium arsenide," *Adv. in Electronics and Electron Physics*, vol. 61, pp. 63-160, Academic Press, New York, 1983.

[30] H. Kressel and J. K. Butler, *Semicondunctor Lasers and Heterojunction LEDs*, pp. 46-47, Academic Press, New York, 1977.

[31] P. Van Halen and D. L. Pulfrey, "Accurate, short series approximations to Fermi-Dirac integrals of order -1/2, 1/2, 1, 3/2, 2, 5/2, 3, and 7/2," *J. Appl. Phys.*,, vol. 57, no. 12, pp. 5271-5274, 1985.

[32] J. S. Blakemore, "Semiconducting and other major properties of gallium arsenide," *J. Appl. Phys.*, vol. 53, no. 10, pp. 123-181, 1982.

[33] R. P. Mertens, R. J. van Overstraeten, and H. J. de Man, "Heavy doping effects in silicon," *Adv. in Electronics and Electron Physics*, vol. 55, pp. 77-118, Academic Press, New York, 1981.

[34] J. S. Blakemore, "Intrinsic density $n_i(T)$ in GaAs: Deduced from band gap and effective mass parameters and derived independently from Cr acceptor capture and emission coefficients," *J. Appl. Phys.*, vol. 53, no. 1, pp. 520-531, 1982.

[35] J. P. Bailbe, A. Marty, and G. Rey, "Influence of degeneracy behaviour of homojunction GaAs bipolar transistor," *Electron. Lett.*, vol. 20, no. 6, pp. 258-259, 1984.

[36] In Reference 30, p. 19.

[37] V. F. Dvoryankin, O. V. Emel'yanenko, D. N. Nasledov, D. D. Nedeoglo, and A. A. Telegin, "Electrical properties of epitaxial films of n-type GaAs," *Sov. Phys.-Semicond.*, vol. 5, no. 10, pp. 1636-1640, 1972.

[38] D. E. Hill, "Activation energy of holes in Zn-doped GaAs," *J. Appl. Phys.*, vol. 41, pp. 1815-1818, 1970.

[39] S. M. Sze, *Physics of Semiconductor Devices*, pp. 22-27, 2nd ed., John Wiley & sons, New York, 1981.

[40] D. E. Hill, "Infrared transmission and fluorescence of doped Gallium Arsenide," *Phys. Rev.*, vol. 133, no. 3A, pp. 866-872, 1964.

[41] O. V. Emel'yanenko, T. S. Lagunova, and D. N. Nasledov, "Scattering of current densities in gallium arsenide in the presence of strong degeneracy," *Sov. Phys.-Solid State*, vol. 2, pp. 176-180, 1960.

[42] T. Katoda and T. Sugano, "Hall effect, Schottky barrier capacitance, and photoluminescence spectra measurements for GaAs epitaxial layer and their correlation," *J. Electrochem. Soc.*, vol. 121, no. 8, pp. 1066-1073, 1974.

[43] W. Walukiewicz, L. Lagowski, L. Jastrzebski, M. Lichtensteiger, and H. C. Gatos, "Electron mobility and free-carrier absorption in GaAs: Determination of the compensation ratio," *J. Appl. Phys.*, vol. 50, no. 2, pp. 899-908, 1979.

[44] H. M. Cox and J. V. DiLorenzo, "Characteristics of an $AsCl_3/Ga/H_2$ two-bubbler GaAs CVD system for MESFET applications," *Gallium Arsenide and Related Compounds* [*Conf. Ser.-Inst. Phys.*], no. 33b, pp. 11-22, 1977.

[45] D. J. Ashen, P. J. Dean, D. T. J. Hurle, J. B. Mullin, A. Royle, and A. M. White, "The incorporation of residual impurities in vapour grown GaAs," *Gallium Arsenide and Related Compounds* [*Conf. Ser.-Inst. Phys.*], no. 24, pp. 229-244, 1975.

[46] F. D. Rosi, D. Meyerhofer, and R. V. Jensen, "Properties of p-type GaAs prepared by copper diffusion," *J. Appl. Phys.*, vol. 31, no. 6, pp. 1105-1108, 1960.

[47] Sh. M. Gasanli, O. V. Emel'yanenko, V. K. Ergakov, F. P. Kesamanly, T. S. Lagunova, and D. N. Nasledov, "Determination of the impurity concentration from the Hall effect and the hole mobility in Zn-doped Gallium Arsenide crystals," *Sov. Phys.-Semicond.*, vol. 5, no. 10, pp. 1641-1644, 1972.

[48] J. Vilms and J. P. Garrett, "The growth and properties of LPE GaAs," *Solid-State Electron.*, vol. 15, pp. 443-455, 1972.

[49] J. Vilms and W. E. Spicer, "Quantum efficiency and radiative lifetime in p-type Gallium Arsenide," *J. Appl. Phys.*, vol. 36, no. 9, pp. 2815-2821, 1965.

[50] W. Walukiewicz, L. Lagowski, L. Jastrzebski, and H. C. Gatos, "Minority-carrier mobility in p-type GaAs," *J. Appl. Phys.*, vol. 50, no. 7, pp. 5040-5042, 1979.

[51] C. Hilsum and B. Holeman, "Carrier lifetime in GaAs," *Proc. Int'l Conf. on Semicond. Phys.*, pp. 962-966, 1960.

[52] R. J. Nelson and R. G. Sobers, "Minority-carrier lifetime and internal quantum efficiency of surface-free GaAs," *J. Appl. Phys.*, vol. 49, no. 12, pp. 6103-6108, 1978.

[53] M. Ettenberg, H. Kressel, and S. L. Gilbert, "Minority carrier diffusion length and recombination lifetime in GaAs:Ge prepared by liquid-phase epitaxy," *J. Appl. Phys.*, vol. 44, no. 2, pp. 827-831, 1973.

[54] G. B. Scott, G. Duggan, and P. Dawson, "A photoluminescence study of beryllium-doped GaAs grown by molecular beam epitaxy," *J. Appl. Phys.*, vol. 52, no. 11, pp. 6888-6894, 1981.

[55] K. L. Ashley and J. R. Biard, "Optical microprobe response of GaAs diodes," *IEEE Trans. Electron Devices*, vol. ED-14, no. 8, pp. 429-432, 1967.

[56] C. J. Hwang, "Doping dependence of hole lifetime in n-type GaAs," *J. Appl. Phys.*, vol. 42, no. 11, pp. 4408-4413, 1971.

[57] L. Lagowski, L. Jastrzebski, and H. C. Gatos, "Application of scanning electron microscopy to determination of surface recombination velocity: GaAs," *Appl. Phys. Lett.*, vol. 27, no. 10, pp. 537-539, 1975.

[58] G. A. Acket and J. J. Scheer, "Relaxation oscillations and recombination in epitaxial n-type Gallium Arsenide," *Solid-State Electron.*, vol. 14, pp. 167-174, 1971.

[59] L. F. Shampine and R. C. Allen Jr., *Numerical Computing : An Introduction*, pp. 87-108, Saunders, Philadelphia, 1973.

[60] A. Neugroschel, M. Arienzo, Y. Komen, and R. D. Isaac, "Experimental study of the minority-carrier transport at the polysilicon-monosilicon interface," *IEEE Trans. Electron Devices*, vol. ED-32, pp. 807-816, 1985.

[61] H. K. Gummel, "A self-consistent iterative scheme for one-dimensional steady state transistor calculations," *IEEE Trans. Electron Devices*, vol. ED-11, no. 10, pp. 455-465, 1964.

[62] A. DeMari, "An accurate numerical steady state one-dimensional solution of the P-N junction," *Solid-State Electron.*, vol. 11, pp. 33-58, 1968.

[63] -------, "An accurate numerical one-dimensional solution of the P-N junction under arbitrary transient conditions," *Solid-State Electron.*, vol. 11, pp. 1021-1053, 1968.

[64] D. L. Scharfetter and H. K. Gummel, "Large-signal analysis of a silicon Read diode oscillator," *IEEE Trans. Electron Devices*, vol. ED-16, no. 1, pp. 64-77, 1969.

[65] J. W. Slotboom, "Iterative scheme for 1- and 2-dimensional D.C.-transistor simulation," *Electron. Lett.*, vol. 5, pp. 677-678, 1969.

[66] H. W. Loeb, R. Andrew, and W. Love, "Application of 2-dimensional solutions of the Shockley-Poisson equation to inversion-layer M.O.S.T. devices," *Electron. Lett.*, vol. 4, pp. 352-354, 1968.

[67] J. E. Schroeder and R. S. Muller, "IGFET analysis through numerical solution of Poisson's equation," *IEEE Trans. Electron Devices*, vol. ED-15, no. 12, pp. 954-961, 1968.

[68] E. M. Buturla, P. E. Cottrell, B. M. Grossman, K. A. Salsburg, M. B. Lawlor, and C. T. McMullen, "Three-dimensional finite element simulation of semiconductor devices," *Proc. Int. Solid-State Circuits Conf.*, pp. 76-77, 1980.

[69] N. Shigyo, M. Konaka, and R. L. M. Dang, "Three-dimensional simulation of inverse narrow-channel effect," *Electron. Lett.*, vol. 18, no. 6, pp. 274-275, 1982.

[70] F. N. Trofimenkoff, "Field-dependent mobility analysis of the field-effect transistor," *Proc. IEEE*, vol. 53, no. 11, pp. 1765-1766, 1965.

[71] V. L. Dalal, A. B. Dreeben, and A. Triano, "Temperature dependence of hole velocity in p-GaAs," *J. Appl. Phys.*, vol. 42, no. 7, pp. 2864-2867, 1971.

[72] W. V. Mclevige, M. J. Helix, W. V. Vaidyanathan, and B. G. Streetman, "Electrical profiling and optical activation studies of Be-implanted GaAs," *J. Appl. Phys.*, vol. 48, no. 8, pp. 3342-3346, 1977.

[73] J. Lindhard, M. Scharff, and H. E. Schiøtt, "Range concepts and heavy ions ranges," *Mat. Fys. Medd. Dan. Vid. Selsk.*, vol. 33, pp. 1-42, 1963.

[74] J. F. Gibbons, W. S. Johnson, and S. W. Mylroie, *Projected Range Statistics,* 2nd ed. Dowden, Hutchinson, and Ross, Stroudburg, Pennsylvania, 1975.

[75] H. Ryssel and I. Ruge, *Ionenimplantation*, Teubner, Stuttgart, 1978.

[76] S. Selberherr and E. Guerrero, "Simple and accurate representation of implantation parameters by low order polynomial," *Solid-State Electron.*, vol. 24, pp. 591-593, 1981.

[77] D. V. Morgan, F. H. Eisen, and A. Ezis, "Prospects for ion bombardment and ion implantation in GaAs and InP device fabrication," *Proc. IEE*, vol. 128, no. 4, pp. 109-130, 1981.

[78] S. K. Ghandhi, *VLSI Fabrication Principles,* pp. 345-346, John Wiley & Sons, 1983.

[79] C. A. Stolte, "Ion implantation and materials for GaAs integrated circuits," in *Semiconductors and Semimetals*, vol. 20, pp. 89-158, Academic Press, 1984.

[80] T. H. Chen and M. S. Shur, "Analytical models of ion-implanted GaAs FET's," *IEEE Trans. Electron Devices*, vol. ED-32, no. 1, pp. 18-27, 1985.

[81] S. G. Liu, E. C. Douglas, C. P. Wu, C. W. Magee, S. Y. Narayan, S. T. Jolly, F. Kolondra, and S. Jain, "Ion implantation of sulfur and silicon in GaAs," *RCA Review*, Vol. 41, pp. 227-262, 1980.

[82] C. L. Anderson and H. L. Dunlap, "Low-temperature annealing behavior of GaAs implanted with Be," *Appl. Phys. Lett.*, vol. 35, no. 2, pp. 178-180, 1979.

[83] In Ref. 78, pp. 643-644.

APPENDIX A

```
C-----------------------------------------------------------------------C
C     This Program is written in structured WATFIV for implementing    C
C     the analytical model.  The program can handle 2 donor levels     C
C     and 3 acceptor levels.                                            C
C                                                                       C
C     Variable Names                                                    C
C                                                                       C
C     Level          Name     Ion Conc. Act. Energy  Degen.            C
C                                                                       C
C     DONOR 1        NAME1    DN1       ENIN1        DG1               C
C     DONOR 2        NAME2    DN2       ENIN2        DG2               C
C     ACCEPTOR 1     NAME3    DN3       ENIN3        DG3               C
C     ACCEPTOR 2     NAME4    DN4       ENIN4        DG4               C
C     ACCEPTOR 3     NAME5    DN5       ENIN5        DG5               C
C                                                                       C
C     LAYER(I) = The name of the Ith semiconductor layer                C
C     WIDTH(I) = The width of the Ith semiconductor region, in          C
C                Microns                                                C
C     T = The temperature in Kelvin                                     C
C     DIEL =Permittivity of GaAs                                        C
C     MO = Electron rest mass in Kg                                     C
C     NI = Dilute intrinsic carrier concentration in cm-3               C
C     CAYT = Boltzmann's constant * temperature                         C
C     Q = Electonic charge in Coulombs                                  C
C                                                                       C
C-----------------------------------------------------------------------C
      CHARACTER*10 NAME1,NAME2,NAME3,NAME4,NAME5,LAYER(3)
      CHARACTER*3 VAR,BIAS
      EXTERNAL FDHF,FD3HF,EXPN
      REAL NCONC,MOB,NETDOP,NETION,JEP,JBNO,JBNW,JCBOP,JGEN,JBREC
      REAL JREC,JB,JC,ME,MH,SUMD(3),NI,NIEFF(3)
      INTEGER COUNT
      DIMENSION ME(3),MH(3),FC(3),FV(3),ETTA(3),FL(3),BGAP(3)
      DIMENSION WIDTH(3),TAU(3),DCONST(3),DIFFL(3),PCONC(3)
      DIMENSION NCONC(3),EMOB(3),PMOB(3),NETDOP(3),CION(3),XXI(3)
      COMMON NAME1,NAME2,NAME3,NAME4,NAME5
      COMMON DN1,DN2,DN3,DN4,DN5
      COMMON DI1,DI2,DI3,DI4,DI5
      COMMON EN1,EN2,EN3,EN4,EN5
      COMMON ENIN1,ENIN2,ENIN3,ENIN4,ENIN5
      COMMON DG1,DG2,DG3,DG4,DG5
      COMMON T,CN,CP,EG,EFME,EFMH,FNC,FNV,CAYT,Q,ETA,XI,MO
      COMMON SUMTD,SUMTA,SUMID,SUMIA,NI
```

```
      DIEL = 13.1 * 8.854E-14
      T=300
      NI=2.0E06
      MO=9.1095E-31
      CAYT=8.6173E-5 * T
      Q = 1.6022E-19
      COUNT=1
C-----------------------------------------------------------------------C
C     Start initialization for each region of transistor.               C
C     ITER = The number of initializations.                             C
C-----------------------------------------------------------------------C
      READ,ITER
      DO 100 KK=1,ITER
      DO 200 I=1,3
      READ 1,LAYER(I),WIDTH(I)
      WIDTH(I)=WIDTH(I) * 1.0E-4
      READ 2,NAME1,DN1,ENIN1,DG1
      READ 2,NAME2,DN2,ENIN2,DG2
      READ 2,NAME3,DN3,ENIN3,DG3
      READ 2,NAME4,DN4,ENIN4,DG4
      READ 2,NAME5,DN5,ENIN5,DG5
1     FORMAT(T1,A11,T15,E10.4)
2     FORMAT(T1,A11,T15,E8.2,T25,E6.1,T35,E6.1)
      IF ( I .EQ. 1) PRINT 3
3     FORMAT ('1')
      PRINT 4, LAYER(I),'PARAMETERS'
4     FORMAT(T28,A11,A10,/)
      PRINT 5,'DOPANT','DENSITY','ACTIVATION ENERGY','DEGENERACY'
5     FORMAT(A10,9X,A10,7X,A17,4X,A10)
C-----------------------------------------------------------------------C
C      Calculate reduction in activation energy                         C
C      SUMTD = Total donor concentration                                C
C      SUMTA = Total acceptor concentration                             C
C      EN's  = Activation energy of each impurity state                 C
C      ENIN's = dilute activation energy of each impurity state         C
C-----------------------------------------------------------------------C
      SUMTD=DN1+DN2
      SUMTA=DN3+DN4+DN5
C
      IF( ENIN1 .GT. 0.0 ) EN1= ENIN1 - (1.90E-8 * SUMTD**0.3333)
      IF( ENIN2 .GT. 0.0 ) EN2= ENIN2 - (1.90E-8 * SUMTD**0.3333)
      IF( ENIN3 .GT. 0.0 ) EN3= ENIN3 - (2.34E-8 * SUMTA**0.3333)
      IF( ENIN4 .GT. 0.0 ) EN4= ENIN4 - (2.34E-8 * SUMTA**0.3333)
      IF( ENIN5 .GT. 0.0 ) EN5= ENIN5 - (2.34E-8 * SUMTA**0.3333)
      IF( ENIN1 .EQ. 0.0 ) EN1= 0.0
      IF( ENIN2 .EQ. 0.0 ) EN2= 0.0
      IF( ENIN3 .EQ. 0.0 ) EN3= 0.0
      IF( ENIN4 .EQ. 0.0 ) EN4= 0.0
      IF( ENIN5 .EQ. 0.0 ) EN5= 0.0
      IF( EN1 .LE.0.0 ) EN1= 0.0
      IF( EN2 .LE.0.0 ) EN2= 0.0
      IF( EN3 .LE.0.0 ) EN3= 0.0
      IF( EN4 .LE.0.0 ) EN4= 0.0
      IF( EN5 .LE.0.0 ) EN5= 0.0
```

```
      IF ( NAME1 .NE. 'DUMMY      ' ) PRINT 6,NAME1,DN1,EN1,DG1
      IF ( NAME2 .NE. 'DUMMY      ' ) PRINT 6,NAME2,DN2,EN2,DG2
      IF ( NAME3 .NE. 'DUMMY      ' ) PRINT 6,NAME3,DN3,EN3,DG3
      IF ( NAME4 .NE. 'DUMMY      ' ) PRINT 6,NAME4,DN4,EN4,DG4
      IF ( NAME5 .NE. 'DUMMY      ' ) PRINT 6,NAME5,DN5,EN5,DG5
6     FORMAT(A12,8X,E10.4,9X,E10.4,8X,E10.4)
      PRINT 7
7     FORMAT('/')
C-----------------------------------------------------------------------C
C      Calculate the energy bandgap of GaAs by relating the             C
C      bandgap narrowing to the effective intrinsic carrier             C
C      concentration.                                                   C
C      EG0 = Intrinsic bandgap of GaAs at room temperature              C
C      EG = Actual bandgap of GaAs                                      C
C      NIEFF= Effective intrinsic carrier concentration, using          C
C             the empirical formulae of Bailbe et al.                   C
C-----------------------------------------------------------------------C
      IF ( I .EQ. 2) THEN DO
         NIEFF(I) = 9.0E05 + 3.38E-3 * SQRT(SUMTA)
         NIEFF(I) = NIEFF(I) - 6.72E05 * ALOG(SUMTA*1.E-17)
      ELSE DO
         NIEFF(I) = 9.0E05 + 3.38E-3 * SQRT(SUMTD)
         NIEFF(I) = NIEFF(I) - 3.47E05 * ALOG(SUMTD*1.E-17)
      END IF
      EG0=1.519-(5.405E-4*T**2)/(T+204)
      EG1=CAYT * ALOG ( NIEFF(I)*NIEFF(I)/NI/NI )
      EG= EG0-EG1
C-----------------------------------------------------------------------C
C      Compute the electron and hole concentration by                   C
C      solving the equation of detailed balance. An initial             C
C      is chosen for the Fermi energy calculation.                      C
C      EF = Lower bound of the interval                                 C
C      EFG = Upper bound of the interval                                C
C      RE = Initial relative error                                      C
C      AE = Absolute error                                              C
C-----------------------------------------------------------------------C
      EF=0.0
      EFG=1.65
      RE=1.E-6
      AE=1.E-6
      CALL ZERO(EF,EFG,RE,AE,IFLAG)
      FL(I) =EF
      IF ( IFLAG .GE. 2 ) THEN DO
       PRINT, 'CONVERGENCE FAILED'
      ELSE DO
      END IF
       A=ALOG10(CN)
       B=ALOG10(CP)
C-----------------------------------------------------------------------C
C       Calculate the electron mobility :                               C
C       If p-type material, assume number of electrons = number         C
C       of holes for mobility calculation.                              C
C          EHFAC = (weak filed Hall factor)**-1                         C
C          RATIO = Electron mobility in p-GaAs/                         C
C                  Electron mobility in n-GaAs                          C
C-----------------------------------------------------------------------C
```

```
      Y = A
      IF( I .EQ. 2) Y = B
      IF ( Y .LT. 14 ) Y = 14.0
      EHFAC = 0.851
      EMOB(I)=-.05355 - 69783.16*Y + 17348.328*Y**2 - 1579.599*Y**3
      EMOB(I)= EMOB(I) +63.03560142*Y**4 - .9353191689*Y**5
      EMOB(I)= EHFAC * EMOB(I)
      RATIO =684.326936722 - 168.174778461*Y + 15.4966483265*Y**2
     $               - 0.633308960591*Y**3 + .00967786832189*Y**4
      IF ( I .EQ. 2 ) EMOB(I)= RATIO *EMOB(I)
C-----------------------------------------------------------------C
C       Calculate the hole mobility:                              C
C       If n-type material, assume hole concentration = electron  C
C       concentration for mobility calculation.                   C
C       PHFAC = (weak field Hall factor)**-1                      C
C-----------------------------------------------------------------C
      Z = B
      PHFAC = 0.80
      IF ( I .EQ. 1 .OR. I .EQ. 3)  Z = A
      PMOB(I)=502511.268 -156107*Z + 19205.6*Z**2 - 1168.926*Z**3
      PMOB(I)= PMOB(I) + 35.20885*Z**4 - .42017908*Z**5
      PMOB(I)= PHFAC*PMOB(I)
C-----------------------------------------------------------------C
C       Computing the minority carrier parameters.                C
C       TAU's = Lifetimes                                         C
C       DCONST's = Diffusion constants                            C
C       DIFFL's  = diffusion lengths                              C
C-----------------------------------------------------------------C
     IF ( I .EQ. 1 .OR. I .EQ. 3)  THEN DO
        IF( CP/FNV .GE. 1.00E-22 ) THEN DO
           C=1+.35355*CP/FNV - 9.9E-3*(CP/FNV)**2
     $        + 4.45E-4*(CP/FNV)**3
        ELSE DO
           C=1 + .35355*CP/FNV - 9.9E-3*(CP/FNV)**2
        END IF
        DCONST(I)=PMOB(I)*CAYT*C
        E= 545.075507209 - 99.5742908474*A + 5.96752406063*A**2
     $          -0.11903779718*A**3
        TAU(I)=10**E
        DIFFL(I)=SQRT(ABS(TAU(I)*DCONST(I)))
     ELSE DO
C
        IF( CN/FNC .GE. 1.00E-22 ) THEN DO
           D=1 + .35355*CN/FNC - (9.9E-3)*(CN/FNC)**2
     $         + 4.45E-4*(CN/FNC)**3
        ELSE DO
           D = 1 + .35355*CN/FNC-(9.9E-3)*(CN/FNC)**2
        END IF
        DCONST(I)=EMOB(I)*CAYT*D
        F= -7.63238159E-6 - 678.5724587 * B + 157.93508506*B**2
     $          -13.7579663247 * B**3 + 0.531235178933 * B**4
     $          - 0.0076716569056 * B**5
        TAU(I)=10**F
      DIFFL(I)=SQRT(ABS(TAU(I)*DCONST(I)))
     END IF
```

```
C-----------------------------------------------------------------C
C       Compute the physical parameters                           C
C-----------------------------------------------------------------C
      SUMID = DI1 + DI2
      SUMIA = DI3 + DI4 + DI5
      SUMD(I) = SUMID
      CION(I) = ABS( SUMID -SUMIA )
      PCONC(I)=CP
      NCONC(I)=CN
      ETTA(I) =ETA
      XXI(I) = XI
      ME(I) =EFME
      MH(I) = EFMH
      FC(I) = FNC
      FV(I) = FNV
      BGAP(I)=EG
      NETDOP(I)=ABS(SUMTD-SUMTA)
200   CONTINUE
C-----------------------------------------------------------------C
C       Print out the device parameters                           C
C-----------------------------------------------------------------C
      IF( COUNT .EQ. 1) THEN DO
       PRINT 8,LAYER(1),LAYER(2),LAYER(3)
8      FORMAT(T43,A10,T58,A4,T70,A7)
       PRINT 9,'SEMICONDUCTOR LAYER WIDTH =',WIDTH(1),WIDTH(2),
     $                                       WIDTH(3)
       PRINT 9,'ENERGY BAND GAP =',BGAP(1),BGAP(2),BGAP(3)
       PRINT 9,'FERMI LEVEL =',FL(1),FL(2),FL(3)
       PRINT 9,'EF - EG / KT =',ETTA(1),ETTA(2),ETTA(3)
       PRINT 9,'-EF /KT =',XXI(1),XXI(2),XXI(3)
       PRINT 9,'EFFECTIVE INTRINSIC CONC =',NIEFF(1),NIEFF(2),
     $                                      NIEFF(3)
       PRINT 9,'EFFECTIVE MASS OF ELECTRON =',ME(1),ME(2),ME(3)
       PRINT 9,'EFFECTIVE MASS OF HOLE =',MH(1),MH(2),MH(3)
       PRINT 9,'EFFECTIVE DENSITY OF ELECTRON STATES =',FC(1),FC(2),
     $                                                  FC(3)
       PRINT 9,'EFFECTIVE DENSITY OF HOLE STATES =',FV(1),FV(2),
     $                                             FV(3)
       PRINT 9,'HOLE CONCENTRATION IN VAL. BAND =',PCONC(1),
     $                                            PCONC(2),PCONC(3)
       PRINT 9,'ELECTRON CONCENTRATION IN COND. BAND =',NCONC(1),
     $                                          NCONC(2),NCONC(3)
       PRINT 9,'ELECTRON MOBILITY =',EMOB(1),EMOB(2),EMOB(3)
       PRINT 9,'HOLE MOBILITY =',PMOB(1),PMOB(2),PMOB(3)
       PRINT 9,'MINORITY CARRIER DIFFUSION CONSTANT =',DCONST(1),
     $                                         DCONST(2),DCONST(3)
       PRINT 9,'MINORITY CARRIER DIFFUSION LENGHT =',DIFFL(1),
     $                                         DIFFL(2),DIFFL(3)
       PRINT 9,'MINORITY CARRIER LIFETIME =',TAU(1),TAU(2),TAU(3)
       PRINT 9,'NET DOPANT DENSITY =',NETDOP(1),NETDOP(2),NETDOP(3)
       PRINT 9,'DENSITY OF IMMOBILE IONS =',CION(1),CION(2),CION(3)
9      FORMAT ('0',A38,3E13.5)
      ELSE DO
      END IF
```

```
C-----------------------------------------------------------------C
C      Calculate the current components and gains of the transistor C
C      in the analytical model                                    C
C      S = Emitter surface recombination velocity                 C
C      VCE = emitter-collector bias voltage                       C
C-----------------------------------------------------------------C
      S = 2.0E06
      VCE = 5.0
      BIAS= 'VBE'
C-----------------------------------------------------------------C
C      Read in the parameter for sensitivity studies              C
C      VAR = The name of the parameter                            C
C      N = The number of parameter values for evaluation          C
C      PARM = The value  of the parameter                         C
C-----------------------------------------------------------------C
      READ 10,VAR
10    FORMAT(A3)
      READ,N
      DO 100 J=1,N
      READ,PARM
      PRINT 11,'TRANSISTOR BIAS VOLTAGES & CURRENT COMPONENTS'
11    FORMAT('1',T15,A50,/)
      IF( VAR .EQ. 'VCE') THEN DO
          VCE=PARM
          PRINT 9,'EMITTER-COLLECTOR VOLTAGE =',VCE
          ELSE DO
      ENDIF
      IF( VAR .EQ. 'NE ') PRINT 9,'EMITTER DOPANT DENSITY =',SUMD(3)
      IF( VAR .EQ. 'NC ') PRINT 9,'COLLECTOR DOP. DENSITY =',SUMD(1)
      IF( VAR .EQ. 'SV ') THEN DO
          S=PARM
          PRINT 9,'SURFACE RECOMB. VEL =',S
          ELSE DO
      ENDIF
      IF( VAR .EQ. 'WB ' ) THEN DO
          WIDTH(2)=PARM*1.0E-4
          PRINT 9,'BASE WIDTH =',WIDTH(2)
        ELSE DO
      ENDIF
      IF( VAR .EQ. 'WE ' ) THEN DO
          WIDTH(3)=PARM*1.0E-4
          PRINT 9,'EMITTER WIDTH =',WIDTH(3)
      ELSE DO
      END IF
      IF( VAR .EQ. 'TE ' ) THEN DO
          TAU(3)=PARM
          DIFFL(3)=SQRT(ABS(TAU(3)*DCONST(3)))
          PRINT 9,'EMITTER LIFETIME =',TAU(3)
      ELSE DO
      ENDIF
      IF( VAR .EQ. 'TB ' ) THEN DO
               TAU(2)=PARM
               DIFFL(2)=SQRT(ABS(TAU(2)*DCONST(2)))
               PRINT 9,'BASE LIFETIME =',TAU(2)
      ELSE DO
      ENDIF
```

```
C-----------------------------------------------------------------C
C      Calculation of various current components in the analytical C
C      model                                                      C
C-----------------------------------------------------------------C
      DO 300 K=1,41
C
      IF (VAR .EQ. 'VCE') BIAS=VAR
      IF( K.EQ.1 ) PRINT 12,BIAS,'JP(-XE)',' JN(0) ',' JN(XB)',
     $               ' JREC  ', ' JGEN  ','JP(XC) ','JN(0)-JN(XB)',
     $               '  GE   ', 'INJ EFF','B T FAC','   JB  ',
     $               '  JC   ', ' BETA  '
12    FORMAT(5X,A3,8X,6(3X,A7,6X),3X,A12,/,6(3X,A7,6X))
C-----------------------------------------------------------------C
C      Set the bias conditions.                                   C
C      VCB = Base-collector voltage                               C
C      VEB = Base-emitter voltage                                 C
C-----------------------------------------------------------------C
      IF( VAR .NE. 'VBE' ) THEN DO
          VEB = 0.02*(K-1) + 0.50
      ELSE DO
          IF( K .LE. 20) VCE = K*0.1/20.
          IF( K .GT. 20 .AND. K .LE. 30) VCE= (K-20)*0.01+0.1
          IF( K .GT. 30 .AND. K .LE. 41) VCE= (K-30)*4.8/11.+0.2
          VEB=PARM
      ENDIF
      IF( K.EQ.1 .AND. VAR .EQ. 'VBE' ) PRINT 9, '      VBE=',VEB
      VCB = VEB-VCE
C-----------------------------------------------------------------C
C      COMPUTATION OF THE BUILT-IN VOLTAGES                       C
C      BEVBI = Base-emitter junction voltage                      C
C      BCVBI = Base-collector junction voltage                    C
C-----------------------------------------------------------------C
      BEVBI = CAYT * ALOG( PCONC(2) / PCONC(3) )
      BCVBI = CAYT * ALOG( PCONC(2) / PCONC(1) )
C
      XE1  = 2*DIEL*(BEVBI-VEB)*CION(2)
      XE2  = XE1/(1.6022E-19*CION(3)*(CION(2)+CION(3)))
      XE   = SQRT( ABS(XE2) )
      XC   = 2*DIEL*(BCVBI-VCB)*CION(2)/(Q*CION(1)*(CION(2)+CION(1)))
      XC   = SQRT( ABS(XC) )
      XBO = 2*DIEL*(BEVBI-VEB)*CION(3)/(Q*CION(2)*(CION(2)+CION(3)))
      XBO = SQRT( ABS(XBO) )
      XBW = 2*DIEL*(BCVBI-VCB)*CION(1)/(Q*CION(2)*(CION(2)+CION(1)))
      XBW = SQRT( ABS(XBW) )
C-----------------------------------------------------------------C
C      WE = Neutral emitter width                                 C
C      WB = Neutral basewidth                                     C
C-----------------------------------------------------------------C
      WE =  WIDTH(3) - XE
      WB =  WIDTH(2) - XBO -XBW
      DVEB = EXPN( VEB/CAYT) - 1.0
      DVCB = EXPN( VCB/CAYT) - 1.0
      EE = EXPN( 2*WE/DIFFL(3) )
      BB = EXPN( 2*WB/DIFFL(2) )
```

```
C-------------------------------------------------------------------C
C      Computation of the emitter back-injected hole current, JEP,  C
C      as given in the model.                                       C
C-------------------------------------------------------------------C
      PXE = PCONC(3) * DVEB
      IF ( S .EQ. 0.0 ) THEN DO
        PY = 2 * PXE * EXPN( WE/DIFFL(3) ) /( EE + 1 )
      ELSE DO
        IF ( S .GT. 1.E10 ) THEN DO
          PY = 0.0
        ELSE DO
          PY = 2 * PXE * EXPN( WE/DIFFL(3) )
          PY = PY / ( S*DIFFL(3)/DCONST(3)*(EE - 1) + (EE + 1) )
        END IF
      END IF
      JEP = Q*DCONST(3)*( PXE*(EE + 1) - 2*PY*EXPN(WE/DIFFL(3)) )
      JEP = JEP /( DIFFL(3) * ( EE - 1 ) )
C-------------------------------------------------------------------C
C      Computation of the electron diffusion currents at the        C
C      base depletion edges, JBN0 and JBNW                          C
C-------------------------------------------------------------------C
      JBNO = DVEB*( BB + 1 ) - DVCB*2*EXPN( WB/DIFFL(2) )
      JBNO = Q*DCONST(2)*NCONC(2)*JBNO /( DIFFL(2) * ( BB - 1 ) )
      JBNW = DVEB*2*EXPN( WB/DIFFL(2) ) - DVCB*( BB + 1 )
      JBNW = Q*DCONST(2)*NCONC(2)*JBNW /( DIFFL(2) * ( BB - 1 ) )
C-------------------------------------------------------------------C
C      Computation of the generation current in the reversed-biased C
C      base-collector junction, JGEN, and the collector leakage     C
C      current JCBOP.                                               C
C-------------------------------------------------------------------C
      JCBOP = Q * DCONST(1) * PCONC(1) / DIFFL(1)
      JGEN = -Q / 2.0 * (XBW+XC) * SQRT( 1. / (TAU(1)*TAU(2)) )
     $       / COSH( 0.5*ALOG(TAU(1)/TAU(2)) )
C-------------------------------------------------------------------C
C      Computation of the recombination current in the forward      C
C      biased emitter-base junction, as given by Choo's equations.  C
C-------------------------------------------------------------------C
      B = EXP(-0.5*VEB/CAYT ) * COSH( 0.5*ALOG( TAU(3)/TAU(2) ) )
      ALPHA = 2 * SINH( 0.5 * ( BEVBI - VEB ) / CAYT )
      AAA = TAU(2) * PCONC(2) /( TAU(3) * NCONC(3))
      GAMMA = SQRT(AAA)+SQRT(1./AAA) + 2*B*COSH( (BEVBI-VEB)/2/CAYT )
      IF ( B .NE. 1.0 ) THEN DO
        IF ( B .LT. 1.0 ) THEN DO
          FCNB = 1/SQRT( 1-B*B ) * ATAN( ALPHA/GAMMA*SQRT( 1-B*B ) )
        ELSE DO
          BBB = ALPHA * SQRT( B*B -1 ) / GAMMA
          FCNB = 1 / SQRT( B*B - 1) * 0.5 * ALOG( (1+BBB)/(1-BBB) )
        END IF
      ELSE DO
        FCNB = ALPHA / GAMMA
      ENDIF
      JREC =Q*SQRT( PCONC(1)*NCONC(1) )*(XBO+XE)*2*SINH(VEB/2/CAYT )
      JREC = JREC*FCNB / ( SQRT( TAU(2)*TAU(3) )*( BEVBI-VEB )/CAYT )
```

```
C-----------------------------------------------------------------C
C      Computation of the base current density, JB, and the      C
C      collector current density, JC.                            C
C-----------------------------------------------------------------C
      JBREC = JBNO - JBNW
      JB = JEP + JBNO - JBNW - JCBOP - JGEN + JREC
      JC = JBNW + JCBOP + JGEN
C-----------------------------------------------------------------C
C      Computation of other transistor parameters.               C
C      BETA = DC transistor gain                                 C
C      EMIEFF = Emitter injection efficiency                     C
C      BTFAC = Base transport factor                             C
C      GE = Emitter Gummel number                                C
C-----------------------------------------------------------------C
      BETA = JC / JB
      EMIEFF=JBNO/(JEP+JBNO+JREC)
      BTFAC=JBNW/JBNO
      PAR1=DIFFL(3)*S/DCONST(3)
      PAR2=WE/DIFFL(3)
      GE=NCONC(3) * DIFFL(3) * NIEFF(3) * NIEFF(3) / DCONST(3)/4.0E12
     $    *(PAR1*SINH(PAR2)+COSH(PAR2)) / (PAR1*COSH(PAR2)+SINH(PAR1))
      GE=Q*4.0E12*DVEB/(JREC+JEP)
      IF( VAR .EQ.'VCE') THEN DO
          PRINT 13, VCE, JEP, JBNO, JBNW, JREC,JGEN,JCBOP,JBREC,
     $              GE, EMIEFF, BTFAC, JB, JC, BETA
      ELSE DO
          PRINT 13, VEB, JEP, JBNO, JBNW, JREC,JGEN,JCBOP,JBREC,
     $              GE, EMIEFF, BTFAC, JB, JC, BETA
      END IF
13    FORMAT(7(E13.6,3X),E13.6,/,6(E13.6,3X),/)
300   CONTINUE
100   CONTINUE
      STOP
      END
C-----------------------------------------------------------------C
C     This function calculates the exponential of the variable x.  C
C     The overflow error is avoided by setting the minimun f(x) to C
C     be 0 for x < -100, and the maximum f(x) to be exp(100) for   C
C     x > 100.                                                     C
C-----------------------------------------------------------------C
      FUNCTION EXPN(X)
         IF ( X.LT.-100.0) THEN DO
            EXPN=0.0
         ELSE DO
            IF ( X.LE.100.0 .AND. X.GE.-100.0) THEN DO
               EXPN=EXP(X)
            ELSE DO
               IF ( X.GT.100 ) THEN DO
                  EXPN=EXP(100)
               ELSE DO
               END IF
            END IF
         END IF
         RETURN
      END
```

```
C-----------------------------------------------------------------C
C      This function evaluates the Fermi-Dirac Integral of order  C
C      3/2 using short series expressions by Van Halen and Pulfrey. C
C-----------------------------------------------------------------C
      FUNCTION FD3HF(X,EXPN)
         IF ( X .LE. 0.0 ) THEN DO
            FD3HF = EXPN(X) - 0.176826*EXPN(2*X) + 0.064772*EXPN(3*X)
     $              - 0.033677*EXPN(4*X) + 0.021353*EXPN(5*X)
     $              - 0.011451*EXPN(6*X) + 0.003032*EXPN(7*X)
         ELSE DO
            IF ( X .GT. 0.0 .AND. X .LE. 4.0) THEN DO
               FD3HF = 0.867200 + 0.765101*X + 0.302693*X**2
     $                 + 0.062718*X**3 + 0.005793*X**4
     $                 + 0.001342*X**5 + 0.953657*X**6
            ELSE DO
               IF ( X .GT. 4.0 ) THEN DO
                  FD3HF = 0.300901*X**2.5 + 1.85581*X**0.5
     $                    + 0.466432*X**(-1.5) + 7.71648*X**(-3.5)
     $                    + 120.535*X**(-5.5) + 800.702*X**(-7.5)
     $                    + 2189.84*X**(-9.5)
               ELSE DO
               END IF
            END IF
         END IF
      RETURN
      END
C-----------------------------------------------------------------C
C      This function evaluates the Fermi-Dirac Integral of order  C
C      1/2 using short series expressions by Van Halen and Pulfrey. C
C-----------------------------------------------------------------C
      FUNCTION FDHF(X,EXPN)
         IF ( X .LE. 0.0 ) THEN DO
            FDHF = EXPN(X) - 0.353568*EXPN(2*X) + 0.192439*EXPN(3*X)
     $             - 0.122973*EXPN(4*X) + 0.077134*EXPN(5*X)
     $             - 0.036228*EXPN(6*X) + 0.008246*EXPN(7*X)
         ELSE DO
            IF ( X .GT. 0.0 .AND. X .LE. 2.0 ) THEN DO
               FDHF = 0.765147 + 0.604911*X + 0.189885*X**2
     $                + 0.020307*X**3 + 0.004380*X**4
     $                + 0.000366*X**5 + 0.000133*X**6
            ELSE DO
               IF ( X .GT. 2.0 .AND. X .LE. 4.0 ) THEN DO
                  FDHF = 0.777115 + 0.581307*X + 0.206132*X**2
     $                   + 0.017680*X**3 + 0.006549*X**4
     $                   + 0.000784*X**5 + 0.000036*X**6
               ELSE DO
                  IF ( X .GT. 4.0 ) THEN DO
                     FDHF = 0.752253*X**(1.5) + 0.928195*X**(-0.5)
     $                      + 0.680839*X**(-2.5) + 25.7829*X**(-4.5)
     $                      + 553.636*X**(-6.5) + 3531.43*X**(-8.5)
     $                      + 3254.65*X**(-10.5)
                  ELSE DO
                  END IF
               END IF
            END IF
         ENDIF
      RETURN
      END
```

```
C-----------------------------------------------------------------C
C     This subroutine calculate the carrier concentration for each  C
C     semiconductor region by solving the equation for charge       C
C     neutrality.  It searches for a zero of the this non-linear    C
C     equation between the given values B and C until the width of  C
C     the interval (B,C) has collapsed to within a tolerance        C
C     specified by the stopping criterion, ABS(B-C) .LE.            C
C     2*(RW*ABS(B)+AE).                                             C
C-----------------------------------------------------------------C
      SUBROUTINE ZERO(B,C,RE,AE,IFLAG)
      CHARACTER*10 NAME1,NAME2,NAME3,NAME4,NAME5,LAYER
      REAL B,C,RE,AE,NIEFF
      INTEGER IFLAG
      COMMON NAME1,NAME2,NAME3,NAME4,NAME5
      COMMON DN1,DN2,DN3,DN4,DN5
      COMMON DI1,DI2,DI3,DI4,DI5
      COMMON EN1,EN2,EN3,EN4,EN5
      COMMON ENIN1,ENIN2,ENIN3,ENIN4,ENIN5
      COMMON DG1,DG2,DG3,DG4,DG5
      COMMON T,CN,CP,EG,EFME,EFMH,FNC,FNV,CAYT,Q,ETA,XI,MO
      COMMON SUMTD,SUMTA,SUMID,SUMIA,NI
      EXTERNAL EXPN,FDHF,FD3HF
      DATA ER/6.0E-8/
      RW=AMAX1(RE,ER)
      IC=0
      ACBS=ABS(B-C)
      A=C
      INDEX = 1
      EF=A
20    ETA=(EF-EG)/CAYT
      XI=-EF/CAYT
C-----------------------------------------------------------------C
C     Compute effective mass of electrons using F-Dirac statistics  C
C-----------------------------------------------------------------C
      AA=(1.38134E-47) *  3.09*CAYT/EG*FD3HF(ETA,EXPN)
      AA=AA + 1.38134E-47*FDHF(ETA,EXPN)
      AA=AA + (6.8135E-46) * EXPN(ETA-.476/CAYT)
      AA=AA + (3.54638E-46) * EXPN(ETA-.284/CAYT)
      X = FDHF(ETA,EXPN)
      EFME=(AA / X )**(2./3.)
C-----------------------------------------------------------------C
C     Compute effective mass of holes using F-Dirac statistics      C
C-----------------------------------------------------------------C
      BB=(1.82164E-47) * 13.3875*CAYT/EG*FD3HF(XI,EXPN)
      BB= BB + (1.82164E-47+3.07395E-46)*FDHF(XI,EXPN)
      Y = FDHF(XI,EXPN)
      EFMH=(BB / Y )**(2./3.)
C-----------------------------------------------------------------C
C     FNC= Density of states in the conduction band                 C
C     FNV= Density of states in the valence band                    C
C     CN = Electron concentration in the conduction band            C
C     CP = Hole concentration in the valence band                   C
C-----------------------------------------------------------------C
      FNC=(5.55446E+60) * (EFME*T)**1.5
      FNV=(5.55446E+60)* (EFMH*T)**1.5
      CN=FNC * FDHF(ETA,EXPN)
      CP=FNV * FDHF(XI,EXPN)
```

```
C-------------------------------------------------------------------C
C     Compute the densities of the ionised impurities               C
C     DNs = Density of dopants                                      C
C     DIs = Ionized dopant concentration                            C
C-------------------------------------------------------------------C
      DI1=0.0
      IF ( NAME1 .NE. 'DUMMY      ' ) THEN DO
        POWER=( EF-EG+EN1)/CAYT
        DI1=DN1/(1. + ( DG1*EXPN(POWER) ))
      ELSE DO
      ENDIF
      IF( EN1 .EQ. 0.0 ) DI1=DN1
      DI2=0.0
      IF ( NAME2 .NE. 'DUMMY      ' ) THEN DO
        POWER=( EF-EG+EN2)/CAYT
        DI2=DN2/(1. + ( DG2*EXPN(POWER) ))
      ELSE DO
      ENDIF
      IF( EN2 .EQ. 0.0 ) DI2=DN2
      DI3=0.0
      IF ( NAME3 .NE. 'DUMMY      ' ) THEN DO
        POWER=( EN3 -EF )/CAYT
        DI3=DN3/(1. + ( DG3*EXPN(POWER) ))
      ELSE DO
      ENDIF
      IF( EN3 .EQ. 0.0 ) DI3=DN3
      DI4=0.0
      IF ( NAME4 .NE. 'DUMMY      ' ) THEN DO
        POWER=( EN4 -EF )/CAYT
        DI4=DN4/(1. + ( DG4*EXPN(POWER) ))
      ELSE DO
      ENDIF
      IF( EN4 .EQ. 0.0 ) DI4=DN4
      DI5=0.0
      IF ( NAME5 .NE. 'DUMMY      ' ) THEN DO
        POWER=( EN5 -EF )/CAYT
        DI5=DN5/(1. + ( DG5*EXPN(POWER) ))
      ELSE DO
      ENDIF
      IF( EN5 .EQ. 0.0 ) DI5=DN5
C-------------------------------------------------------------------C
C     TEST is the charge neutrality equation. In this subroutine,   C
C     The Fermi energy is computed by iterations until TEST has     C
C     become very small.                                            C
C-------------------------------------------------------------------C
      TEST=(CN+DI3+DI4+DI5)-(CP+DI1+DI2)
C-------------------------------------------------------------------C
C     The following perform the iterations to find the value        C
C     of the Fermi Energy until the stopping criterion is           C
C     reach.                                                        C
C-------------------------------------------------------------------C
      IF ( INDEX .EQ. 1 ) GO TO 30
      IF ( INDEX .EQ. 2 ) GO TO 40
      IF ( INDEX .EQ. 3 ) GO TO  8
30    FA = TEST
      INDEX = 2
```

```
      EF = B
      GO TO 20
40    FB=TEST
      FC=FA
      KOUNT=2
      FX=AMAX1(ABS(FB),ABS(FC))
1     IF ( ABS(FC) .GE. ABS(FB) ) GO TO 2
      A=B
      FA=FB
      B=C
      FB=FC
      C=A
      FC=FA
2     CMB=0.5*(C-B)
      ACMB=ABS(CMB)
      TOL=RW*ABS(B)+AE
      IF ( ACMB .LE. TOL ) GO TO 10
      P=(B-A)*FB
      Q=FA-FB
      IF ( P .GE. 0. ) GO TO 3
      P=-P
      Q=-Q
3     A=B
      FA=FB
      IC=IC+1
      IF ( IC .LT. 4 ) GO TO 4
      IF ( 8.*ACMB .GE. ACBS ) GO TO 6
      IC=0
      ACBS=ACMB
4     IF ( P .GT. ABS(Q)*TOL ) GO TO 5
      B=B+SIGN(TOL,CMB)
      GO TO 7
5     IF ( P .GE. CMB*Q ) GO TO 6
      B=B+P/Q
      GO TO 7
6     B=0.5*(C+B)
7     INDEX = 3
      EF = B
      GO TO 20
8     FB=TEST
      IF ( FB .EQ. 0. ) GO TO 11
      KOUNT=KOUNT+1
      IF ( KOUNT .GT. 200) GO TO 15
      IF ( SIGN(1.0,FB) .NE. SIGN(1.0,FC ) ) GO TO 1
      C=A
      FC=FA
      GO TO 1
10    IF ( FB*FC .GT. 0. ) GO TO 13
      IF ( ABS(FB) .GT. FX ) GO TO 12
      IFLAG=1
      RETURN
11    IFLAG=2
      RETURN
12    IFLAG=3
      RETURN
13    IFLAG=4
```

```
      RETURN
15    IFLAG=5
      RETURN
      END
C-----------------------------------------------------------------------C
C     The following is a typical input file containing data needed      C
C     in the program.  The doping levels and widths in the emitter,     C
C     base, and collector are the typiacal values used in the           C
C     analytical model.  In this case, a sensitivity study of the       C
C     effect of surface recombination velocity of 10**4 and 10**6       C
C     cm/sec on the transistor gain is intended.                        C
C-----------------------------------------------------------------------C
/DATA
1
COLLECTOR     2.0
N-DOPANT      1.00E+16  0.0058    2.0
DUMMY         0.0       0.0       0.0
DUMMY         0.0       0.0       0.0
DUMMY         0.0       0.0       0.0
DUMMY         0.0       0.0       0.0
BASE          0.40
DUMMY         0.0       0.0       0.0
DUMMY         0.0       0.0       0.0
BERYLLIUM     1.00E+17  0.0195    4.0
DUMMY         0.0       0.0       0.0
DUMMY         0.0       0.0       0.0
EMITTER       0.25
DUMMY         0.0       0.0       0.0
SELENIUM      1.00E+17  0.0058    2.0
DUMMY         0.0       0.0       0.0
DUMMY         0.0       0.0       0.0
DUMMY         0.0       0.0       0.0
SV
2
1.0E4
1.0E6
```